GA-A13021
UC-77 Gas Cooled
Reactor Technology

GAS-COOLED FAST BREEDER REACTOR

QUARTERLY PROGRESS REPORT

FOR THE PERIOD FEBRUARY 1, 1974 THROUGH APRIL 30, 1974

by

Project Staff

Prepared for the
U.S. Atomic Energy Commission
San Francisco Operations Office
Under
Contract AT(04-3)-167
Project Agreement No. 23

General Atomic Project 393

June 14, 1974

GENERAL ATOMIC

GENERAL ATOMIC COMPANY
P.O. BOX 81608
SAN DIEGO, CALIFORNIA 92138

PROGRESS REPORT SERIES

GA-5537	November 1, 1963 to July 31, 1964
GA-6667	August 1, 1964 to July 31, 1965
GA-7645	August 1, 1965 to July 31, 1966
GA-8107	August 1, 1966 to July 31, 1967
GA-8787	August 1, 1967 to July 31, 1968
GA-8895	August 1, 1968 through October 31, 1968
GA-9229	November 1, 1968 through January 31, 1969
GA-9359	February 1, 1969 through April 30, 1969
GA-9639	May 1, 1969 through July 31, 1969
GA-9811	August 1, 1969 through October 31, 1969
GA-9838	November 1, 1969 through January 31, 1970
GA-10517	February 1, 1970 through January 31, 1971
GA-10645	February 1, 1971 through April 30, 1971
GA-A10803	May 1, 1971 through July 31, 1971
GA-A10906	August 1, 1971 through October 31, 1971
GA-A12003	November 1, 1971 through January 31, 1972
GA-A12165	February 1, 1972 through April 30, 1972
GA-A12252	May 1, 1972 through July 31, 1972
GA-A12421	August 1, 1972 through October 31, 1972
GA-A12530	November 1, 1972 through January 31, 1973
GA-A12635	February 1, 1973 through April 30, 1973
GA-A12728	May 1, 1973 through July 31, 1973
GA-A12824	August 1, 1973 through October 31, 1973
GA-A12894	November 1, 1973 through January 31, 1974

ABSTRACT

The tasks of the Gas-Cooled Fast Breeder (GCFR) program that are supported by the U.S. Atomic Energy Commission are program planning, component development, reactor system safety, core development, out-of-pile heat-transfer and fluid-flow tests, development of a pressure-equalization system for fuel rods, thermal shielding, fuels and materials development, and nuclear analysis and reactor physics.

The core development task is to establish criteria for the design of the GCFR fuel, control, and blanket element assemblies. Analytical methods are being developed for predicting fuel-rod response to transient conditions and for treating thermal-hydraulic and structural analyses of fuel assemblies. Planning of the test program and test facility for the heat-transfer and fluid-flow tests of fuel assemblies continued. The development work on the pressure-equalization system included obtaining the test assemblies for static adhesion tests and seal leakage tests of mating parts, development of an analytical model for designing monitoring instrumentation, and development of the fuel-rod manifold. In the fuels and materials task, the status of the thermal- and fast-flux irradiation programs and analyses of data from these experiments is given. Plans are being formulated for an in-pile loop test program. Nuclear analysis and reactor physics work included planning and analytical work for a GCFR critical experiment, surveillance of LMFBR critical assembly experiments, and analytical methods development.

CONTENTS

Figures

Tables

1. INTRODUCTION

The Gas-Cooled Fast Breeder Reactor (GCFR) program sponsored by the U.S. Atomic Energy Commission consists of the following tasks: Task 1000—Program Planning, Tasks 2100/2200—Primary Coolant System Components and Prestressed Concrete Reactor Vessel, Task 2700—Reactor System Safety, Task 4100—Core Development, Task 4120—Fuel- and Blanket-element Assemblies, Task 4160—Pressure Equalization System for Fuel, Task 4170—Thermal Shielding, Tasks 4200/4400—Fuels and Materials Development, and Task 4700—Nuclear Analysis and Reactor Physics.

The GCFR Utility Program, which is supported by a large number of electric utility companies, rural electric cooperatives, and General Atomic Company, is primarily directed toward the development of a GCFR demonstration plant. This utility-sponsored work and the AEC-sponsored work are complementary.

1.1. TASK 1000—PROGRAM PLANNING

This task is primarily to coordinate the planning and implementing of the tasks for the technical development of the GCFR. This task also includes liaison with the U.S. Atomic Energy Commission, Argonne National Laboratory (ANL), and Oak Ridge National Laboratory (ORNL).

This task is primarily administrative and thus only the technical work performed on the program during this period is covered in this quarterly report.

1.2. TASKS 2100/2200—PRIMARY COOLANT SYSTEM COMPONENTS AND PRESTRESSED CONCRETE REACTOR VESSEL

The primary coolant system comprises the steam generators, the main helium circulators, ducts and valves, and the core auxiliary cooling system, all of which are enclosed in the prestressed concrete reactor vessel (PCRV). Although based on technology developed for the High-Temperature

Gas-Cooled Reactor (HTGR), the design of the GCFR components will extend this technology to GCFR operating conditions, primarily the higher coolant operating pressure. The design of the PCRV is directly related to the loop components designs and the coolant operating pressures.

The initial work on these tasks will be to review and revise the development program plans presented in the overall GCFR Development Program Plan[1] for these components to reflect the changes in design and program requirements since the plan was prepared.

As the initial phases of these tasks is the review and updating of the development program plans and the preparation of program plan documents for the steam generator, main helium circulator, and the PCRV, the current work on these tasks is not covered in a separate section of this report.

1.3. TASK 2700—REACTOR SYSTEM SAFETY

An analytical study of the reactor safety aspects of the GCFR is to be carried out under this task. Probabilistic methods will be employed to determine and examine risks associated with various accident initiation and progression sequences and thus to identify improvements to the system to reduce such risks.

The initial work on this task is to develop a methodology for analyzing accident progression sequences, which will be carried out in conjunction with the Accident Initiation and Progression Analysis (AIPA) task for the High-Temperature Gas-Cooled Reactor.

1.4. TASK 4100—CORE DEVELOPMENT

The objective of this task is the engineering development of the reactor core and associated components. The work on this task is directed specifically to establishing criteria for the design of the fuel- and blanket-element assemblies. The various analytical and experimental investigations being carried out on this task are reported in Section 3.

Analytical work on fuel-rod behavior under irradiation conditions in a fast flux is now continuing with the LIFE-III code. The uncalibrated version of LIFE-III was received and made operational on the GA computer system.

In the analysis of fuel- and blanket-element assemblies, analytical work is being carried out under subcontract by Battelle Pacific Northwest Laboratories on fuel-rod–spacer interactions. This work consists of structural analyses of the spacer grid for several loading conditions imposed by the fuel rod, such as fuel-rod bowing and irradiation-induced swelling and creep. Both lateral loads and friction-induced axial loads are being investigated. Spacer-grid models are being developed for this analytical work.

Thermal and irradiation distortion of the fuel-element duct is being studied.

The temperature of the duct is affected by the coolant temperature and flow within the ducts, the insulating effect of the spacer-grid hanger straps on the inner duct wall, the bypass flow of coolant around the hanger straps, and the recirculating flow outside the ducts. The coolant flow between elements and the coolant bypass flow behind the spacer-grid hangers are being analyzed for the subsequent analysis of duct temperatures.

Experiments are being carried out to determine the range of H_2 and H_2O impurities in the GCFR helium coolant within which the interaction of fuel rods and spacer grids will be satisfactory during power operation. Fuel-rod cladding tubes and spacers of various types of material are being tested in a helium atmosphere with various H_2-to-H_2O ratios.

1.5. TASK 4120—FUEL- AND BLANKET-ELEMENT ASSEMBLIES

A series of out-of-pile heat-transfer and fluid-flow tests are to be performed to demonstrate the ability of the GCFR fuel, control, and blanket element designs to meet design goals and to verify predictions of analytical models that describe design operation and accident behavior. The test emphasis will be to obtain thermal-structural data for steady-state, transient, and margin conditions using electrically heated rod bundles in a dynamic helium loop. The work currently being carried out on this task is the planning for a helium-loop test series and the development of a test facility. This program is to be carried out jointly by GA and ORNL.

A test program plan based on the selected rod-bundle sizes is being prepared, as discussed in Section 4.

1.6. TASK 4160—PRESSURE EQUALIZATION SYSTEM FOR FUEL

The objective of this task is to develop a system for equalizing the pressure between the inside and the outside of the GCFR fuel rod and for venting the fission products via a trapping system and an instrumented activity monitoring system to a helium purification system. The work performed on this task during this reporting period is presented in Section 5.

In the test program for developing the element-to-grid-plate and vent-connection seal, a two-part test program is to be carried out: (1) a materials screening test for determining static adhesion of mated fuel-element and grid-plate parts and (2) leakage tests of vent connection seals. Procurement, fabrication, and assembly of test apparatus and test parts are in progress for both the static adhesion tests and the seal leakage tests.

Analysis of the monitoring system for the pressure-equalization system is being carried out to obtain design information for a system of stations and instrumentation that will monitor the activity passing from the fuel and blanket elements to the helium purification system. A Ge(Li) analyzer system is being designed using the computer program COUNT, which is being developed as a monitor-instrumentation design tool. The program will be verified using measured data taken from the capsule GB-10 irradiation experiment using a Ge(Li) detector that has been installed on the gas-sampling line by ORNL.

In the development of a fission-product manifold and fuel-rod support for the fuel elements, four manifold designs are currently being evaluated to determine their amenability to fabrication and inspection. In addition, several types of connections for attaching the fuel rods to the manifold are being investigated.

1.7. TASK 4170—THERMAL SHIELDING

The GCFR thermal shield development program will include analytical and experimental tasks to establish the integrity and performance of the shielding materials under anticipated GCFR operating conditions. The experimental program will verify performance, predictions of radiation attenuation, internal heat generation, heat-removal capabilities, and longevity

and integrity of the proposed shielding materials. The work to date on this task is discussed in Section 6.

1.8. TASK 4200/4400—FUELS AND MATERIALS DEVELOPMENT

The fuels and materials development and testing program extends and applies Liquid-Metal Fast Breeder Reactor (LMFBR) fuel technology to GCFR requirements. This task includes surveillance of the LMFBR fuels and materials program to utilize existing and developing technology applicable to the GCFR. The status of the GCFR thermal-flux and fast-flux irradiation test programs is presented in Section 7.

The postirradiation examination and analyses of the charcoal trap from capsule GB-9 have been completed. Preparations have been started on a summary report.

Irradiation capsule GB-10 has achieved a burnup of 43,000 MWd/Te, of which 27,000 MWd/Te was achieved at 12.0 kW/ft at a maximum cladding outside temperature of 565°C and 16,000 MWd/Te was at 13.5 kW/ft and a maximum cladding outside temperature of 630°C. Irradiation of capsule GB-10 is continuing at ORNL to an exposure goal of 75,000 MWd/Te.

Studies of the effect of pressure level on the active fission-product gases released are being carried out. Capsule GB-10 was operated at 200 psi (versus normal operation at 1000 psi) for ∿5,000 MWd/Te. It is currently being operated at 300 psi for an additional exposure of ∿5,000 MWd/Te. After power-cycling and depressurization testing, the power will be increased to 14.8 kW/ft.

Planning for tritium monitoring in capsule GB-10 is continuing.

Irradiation of the seven-fuel-rod capsule experiment F-1 (X094B) had reached a burnup exposure of 70,000 MWd/Te up to the time the EBR-II was shut down for annual maintenance. The F-1 experiment will continue to a burnup goal of 100,000 MWd/Te on the remaining initial fuel rod (G-4).

Destructive and nondestructive examination of the five fuel rods removed during the second interim examination at 50,000 MWd/Te is continuing at Argonne (ANL). Examination of rod G-1, which operated at a maximum

outside cladding temperature of ∿800°C to a burnup of ∿56,000 MWd/Te, indicates that the diametral strain was no more than 0.3% and that the cladding attack was no more than 2.5 mils in depth.

Analysis of gamma-scanning data taken during the second interim examination is continuing. The study of fission-product transport in the F-1 fuel rods is concentrated on four nuclides: Zr^{95}, Cs^{137}, I^{131}, and Ba^{140}/La^{140}.

The preparation of the capsules and fuel rods for the F-3 experiment is continuing. The assembly of the 12 fuel rods was completed and encapsulation and sodium-bonding has been initiated.

In support of the GCFR fuel-element development program, an in-pile loop test program is being planned. The in-pile loop tests will provide the information necessary to establish design and safety margins of the fuel elements and verify the analytical methods developed.

A scoping study to define costs and schedules for this program has been initiated. Aerojet General Nuclear Corporation (ANC) will prepare the scoping study. Major portions of tradeoff studies for the loop and a test reactor evaluation were completed by ANC. A preliminary draft of the management plan was prepared by GA.

1.9. TASK 4700—NUCLEAR ANALYSIS AND REACTOR PHYSICS

This task involves the surveillance and analyses of LMFBR physics work and critical experiments to properly coordinate and develop a GCFR nuclear analysis and physics program and the design and planning of a GCFR critical experiment program. The work performed under this task during this reporting period is discussed in Section 8.

A sequence of six program phases has been proposed for the GCFR critical experiment program, which is planned to begin in the second quarter of FY-75 in the ZPR-9 facility. The six phases progress from a single large core with uniform "average" enrichment and correct void fraction to a four-zone core.

Preliminary analysis at GA has been directed towards benchmark calculations for Phase I of Assembly 1. Two separate two-region cell calculations were performed to account for resonance energy shielding effects. In addition, eigenvalue calculations were made to determine the critical radius for the benchmark core with no streaming corrections.

An initial series of calculations was made to simulate steam entry in the Phase I critical assembly. Two-region spectral calculations have been made using H_2O and H_2C to simulate steam.

REFERENCE

1. "Gas-Cooled Fast Breeder Reactor Demonstration Plant Development Program Plan," USAEC, Report Gulf-GA-A10788, Gulf General Atomic, September 20, 1972.

2. TASK 2700—REACTOR SYSTEM SAFETY

An analytical study is to be carried out of the reactor safety aspects of the GCFR by employing probabilistic methods to determine and examine risks associated with various accident initiation and progression sequences and to identify potential improvements to the system to reduce such risks. For this study, a logical methodology will be developed for the analysis of accident progression sequences in conjunction with the Accident Initiation and Progression Analysis (AIPA) task for the High-Temperature Gas-Cooled Reactor. The developed methodology will be applied in increasing levels of detail to the analysis of selected accident sequences for the GCFR.

Previous work relating to Accident Initiation and Progression Analysis was reviewed, and an interface with the HTGR AIPA program has been established to jointly develop an AIPA analytical method. Current work involves an evaluation of the method in the analysis of a sample problem—the loss of all offsite power.

3. TASK 4100—CORE DEVELOPMENT

3.1. FUEL- AND BLANKET-ROD ANALYSIS

Participation in the LIFE Fuels Properties and Model Working Group continued. The uncalibrated version of the LIFE-III code was received at the end of the quarter and was made operational on the GA computer system. Analysis of GCFR irradiation experiments was initiated.

3.2. ANALYSIS OF FUEL- AND BLANKET-ELEMENT ASSEMBLIES

3.2.1. Analysis of Fuel-rod—Spacer Interaction

A structural analysis is being made of the spacer-grid structure for several loading conditions imposed on the spacer grid by the fuel rods. These loads result from fuel-rod bowing, which is due to temperature gradients across the rods, and from irradiation-induced swelling and creep. They consist of both lateral loads and friction-induced axial loads that develop when the rod moves relative to the grid. The principal effort on this subtask is being performed by Battelle Pacific Northwest Laboratories under a subcontract.

3.2.1.1. Axial Spacer-grid Loading. The analysis of axial loading is to determine the deflections of the fuel-rod grid support structure resulting from a sudden axial relative movement of the fuel rods. This movement will occur during a thermal transient caused by a sudden reduction in reactor power. It is envisioned that the cause of this type of motion would be the result of a normal reactor trip condition. The potential for this type of loading exists within the normal operation of the reactor system.

The motion of the reactor fuel rods relative to the support grids can cause a transverse grid load limited by friction. The friction load will limit the peak load to the breakaway coefficient of static friction that can be developed. The limiting case for this load would be for a friction

coefficient sufficiently large that the breakaway or a limiting load is not reached. For this condition, the grid follows the motion of the fuel rod and the deflection of the grid is controlled directly by the integrated displacements of the rods as opposed to the uniform load previously used.

The initial analysis was based on the assumption of 1.0-lb axial load per rod, which results from a maximum of 1.0 lb/rod normal loading and a coefficient of friction of 1.0. This load was derived from analyses of fuel-rod bowing using the CRASIB code; the coefficient of friction is derived from experimental data (see Section 3.3). The geometrical considerations are based on an electrodischarge-machined (EDM) grid. The EDM grid is the most straightforward grid to analyze in terms of the complexity of the model needed to adequately represent it. The grid has well-defined nodal boundaries and has a uniform thickness. Because of these properties, this type of grid adequately represents an assemblage of beam elements.

The actual model used was a quarter segment of the EDM grid. It is composed of 225 elements and 165 nodes and represents 67.75 rod locations. The deflection solution was based on 1.0 lb/rod load, which means a total axial loading of 67.75 lb. This load is applied to each nodal point, assuming an effective 1.0-lb load per unit cell or rod. The grid model is shown in Figs 3.1 and 3.2.

The results show that the peak bending stresses caused by this loading occur in the second and third row from the center rod. These bending stresses approach 4400 psi for the 1.0 lb/rod applied load. The bending stresses in the beam elements of the grid that are oriented in the tangential direction attain similar intensities as those in the beam elements in the radial direction (see Figs. 3.3 and 3.4).

The deflections shown in Fig. 3.5 are computed for a load of 1.0 lb/rod. The associated stress distribution for larger deflections are not a linear function of displacements. Further work is planned to investigate the effects of geometric nonlinearity on the beam element stress and deflections.

Based on a linear extrapolation of results, it appears that a yield condition in the web material will be reached before local buckling is obtained (see Fig. 3.6). This is based on using a web depth of 0.75 in. and 20% cold-worked Type 316 stainless steel for the material.

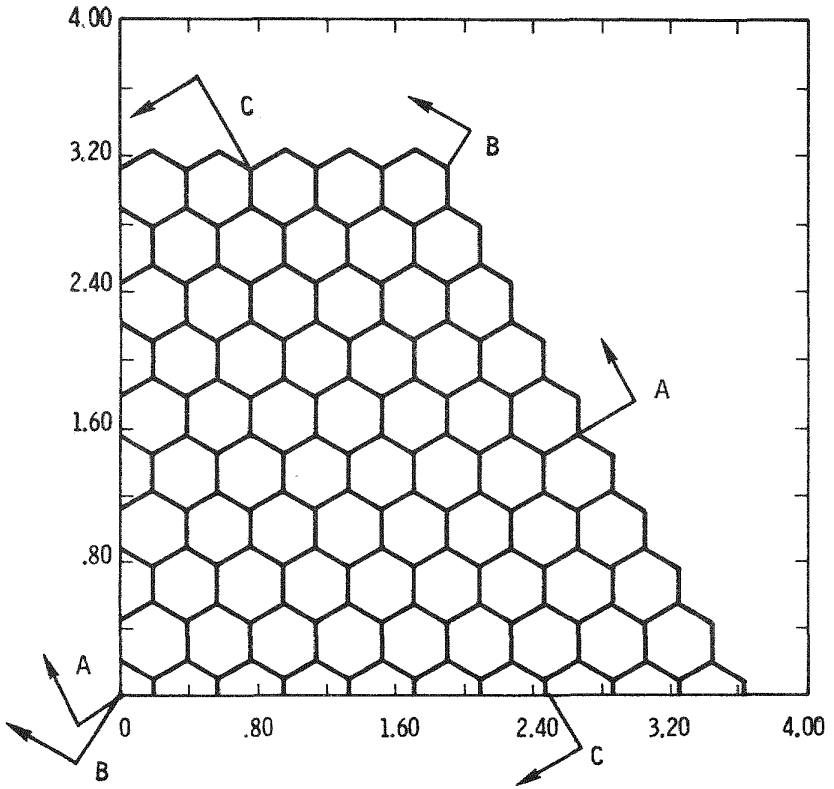

Fig. 3.1 Plan view of spacer-grid model

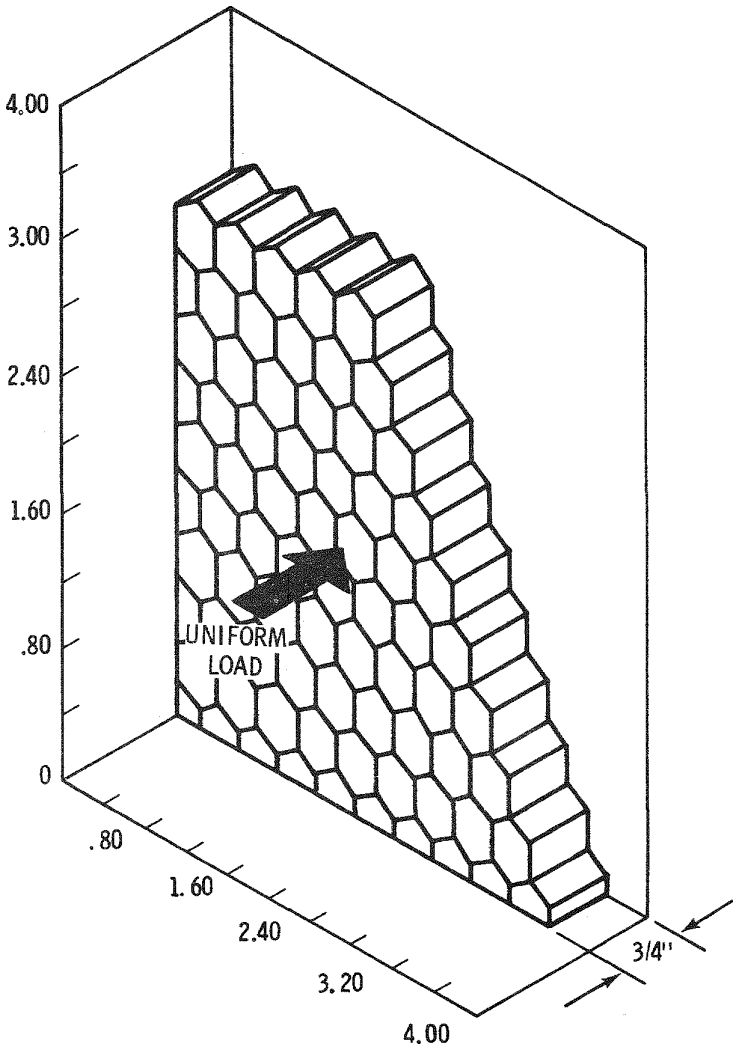

Fig. 3.2 Isometric view of spacer-grid model

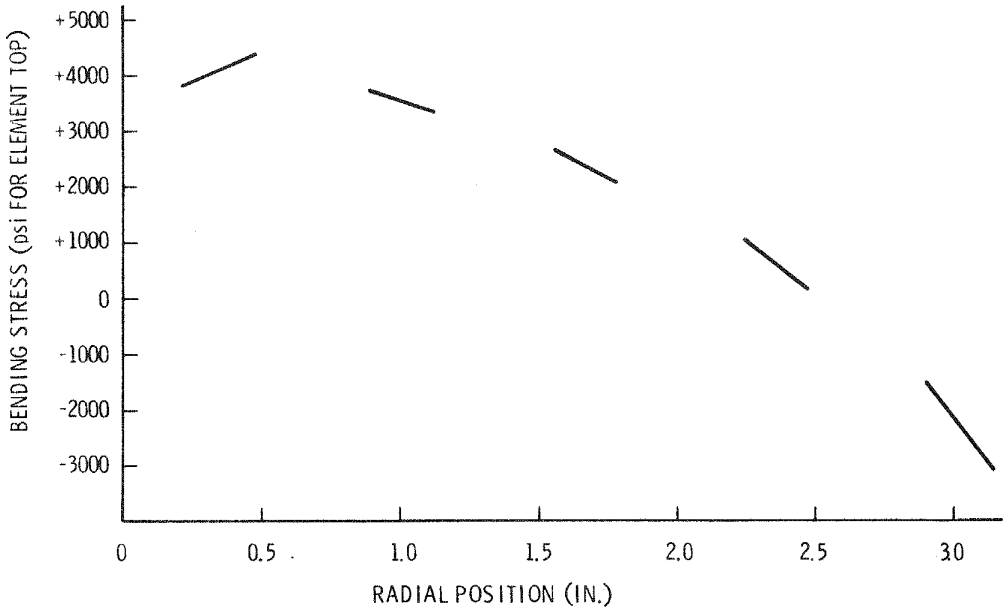

Fig. 3.3 Bending stress in cell web vs. position from grid center (see section A-A of grid layout in Fig. 3.1)

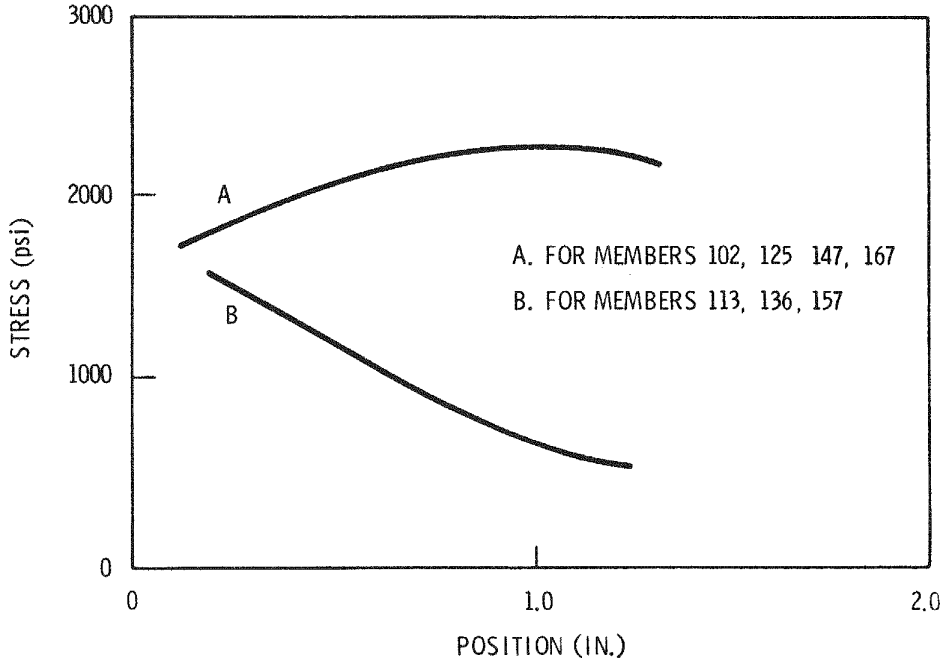

Fig. 3.4 Typical grid tangential average bending stress (normal to section A-A on section line C-C)

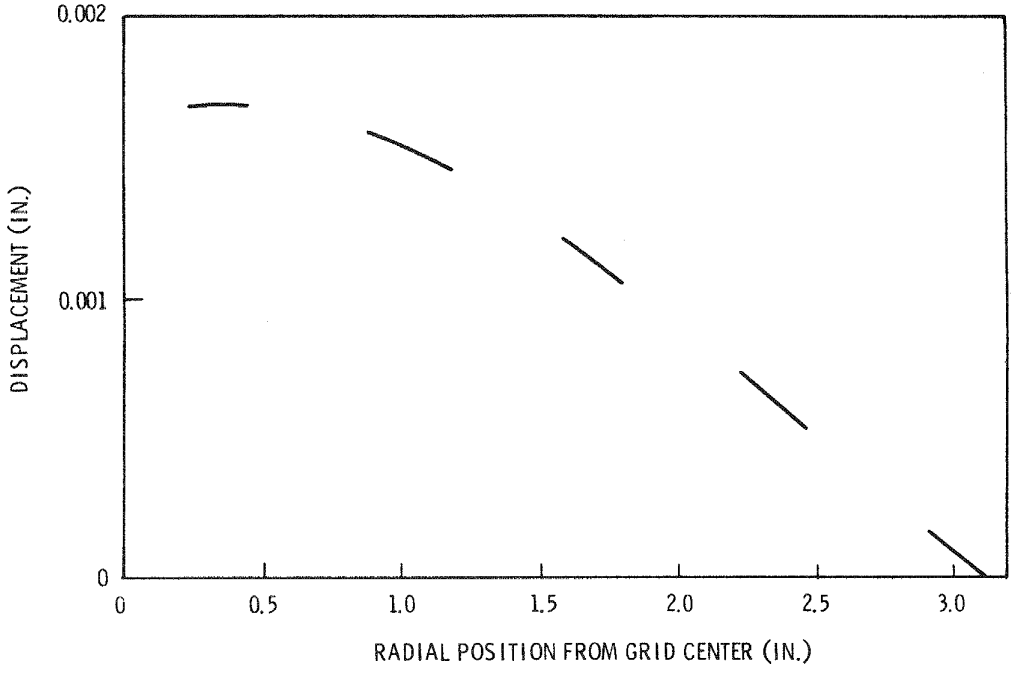

Fig. 3.5 Transverse deflection for 30° traverse from grid center for 1 lb/rod load (see section A-A of grid layout in Fig. 3.1)

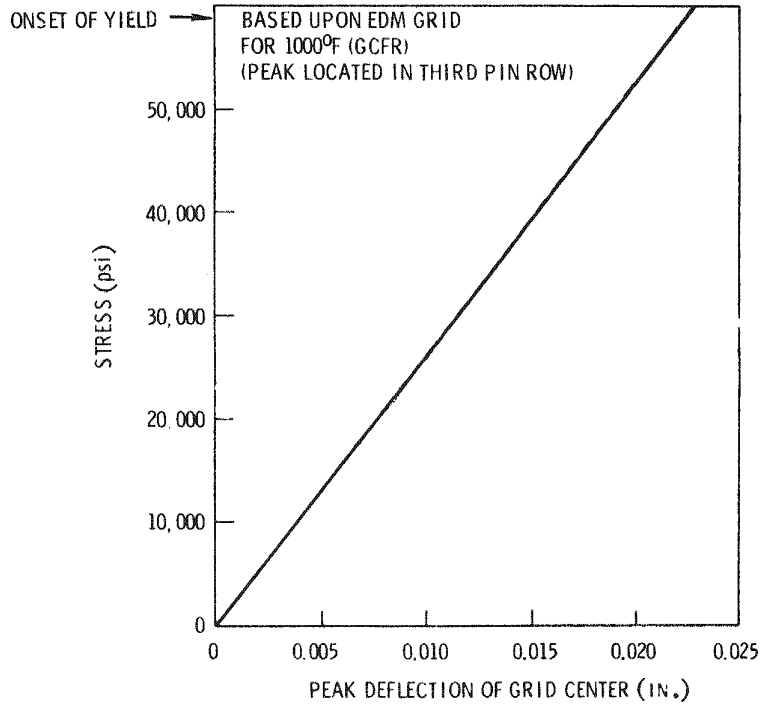

Fig. 3.6 Peak bending stress in grid vs. peak center deflection

Using a grid depth of 0.75 in. and the cell rotations obtained from the application of the uniform unit load, an estimate of the maximum allowable deflection can be made. It is assumed that the limiting case on grid deflection consists of the reduction of the inscribed circle diameter in the rod unit cell to the tolerance on that cell. For this case, the diametral clearance of 0.0045 in. was used, which resulted in a limiting load of 20 lb/rod or a center deflection of approximately 0.030 in. For deflections greater than this amount, the possibility of the rod being subjected to two planar contacts exists.

3.2.1.2. Spacer-grid Unit Cell Distortion. The purpose of this analysis is to determine the deflection of a unit cell in the EDM grid lattice structure. The analysis has been performed for three separate grid models. The approach used has been to evaluate the general overall stiffness by using beam elements of several interacting element walls. A more refined approach was then used to investigate the deflection of one cell wall with a dimple present. This work was performed using plate elements to characterize the dimple region. In order to investigate the dimple and possible variations in design, two plate element models were used.

The conceptual model and the deflected shape after 18,000 hr is shown in Fig. 3.7. The creep deflection was very small compared with the initial elastic deflection. This was due to the very low stress levels that were present in the structure. Peak bending stresses in the beam elements were found to be less than 2,400 psi at the cell center. The associated peak displacements were found to be 0.6×10^{-4} in. for a 1.0-lb load.

The analysis of the grid cell using the plate element models is outlined in Figs. 3.8 through 3.10. For this approach, the prime interest was in the magnitude that the local deflections and stresses actually assume. From the analysis performed to date, the peak stresses that occur in the dimple are less than 4,000 psi. The creep deflection of this cell structure model also appears to be negligible.

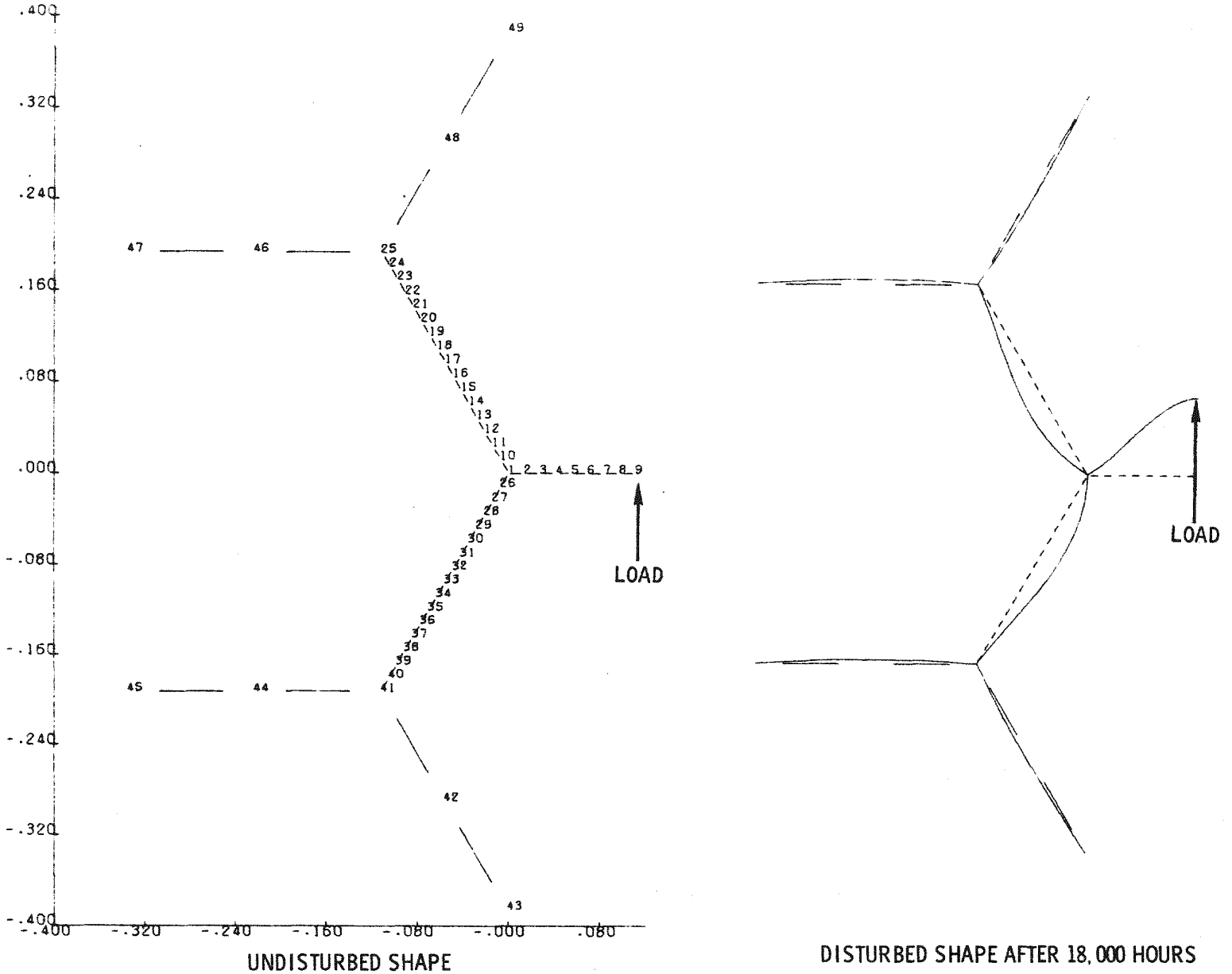

UNDISTURBED SHAPE

DISTURBED SHAPE AFTER 18,000 HOURS

Fig. 3.7 Unit cell fuel-rod spacer model

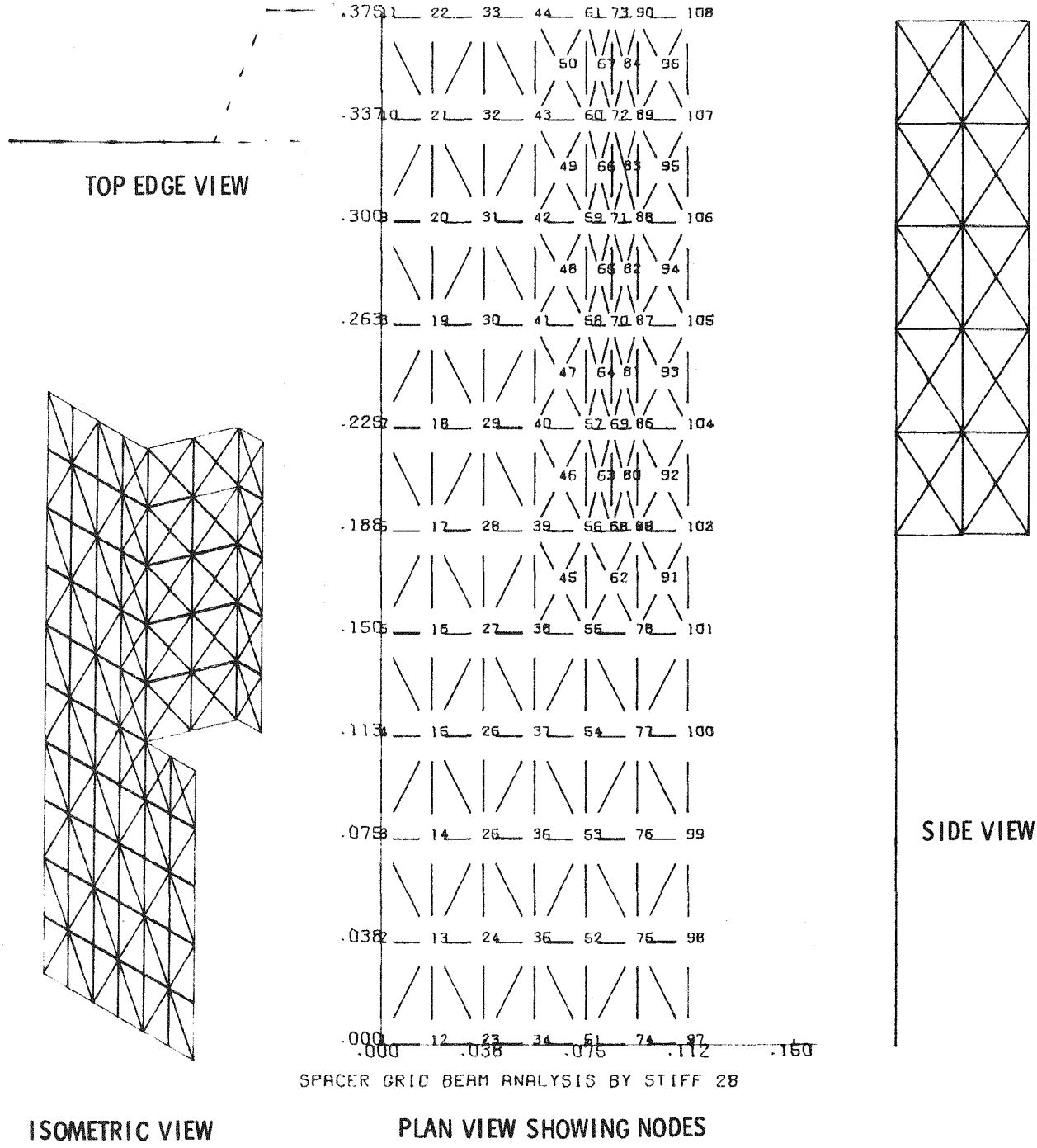

Fig. 3.8 Dimple model with square end

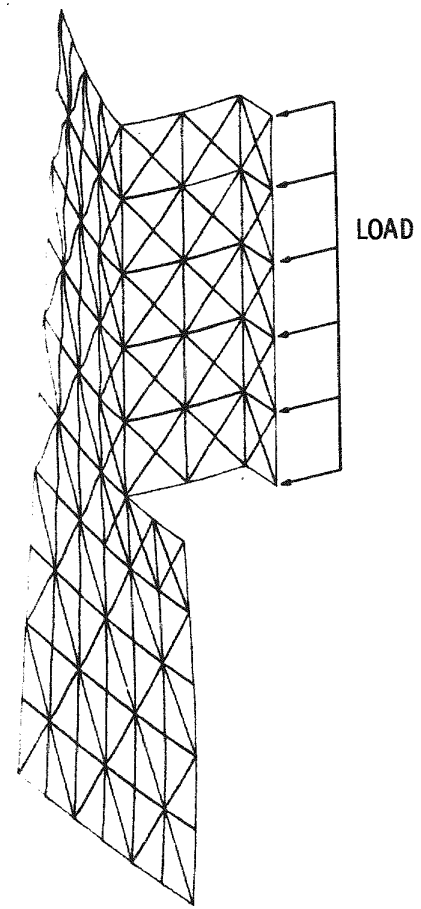

ISOMETRIC VIEW DEFLECTED

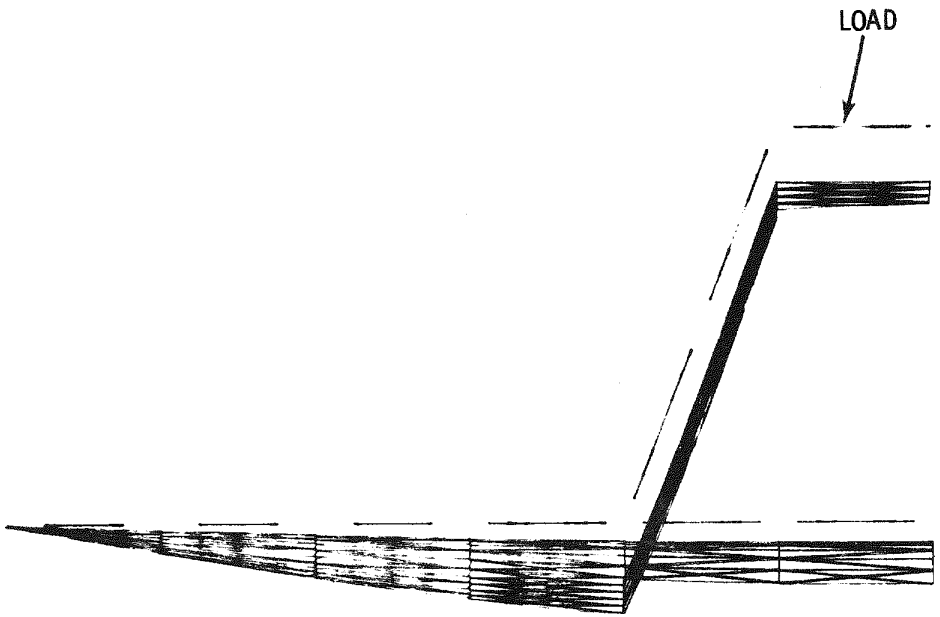

PLAN VIEW DEFLECTED

Fig. 3.9 Deflection of square-ended dimple model

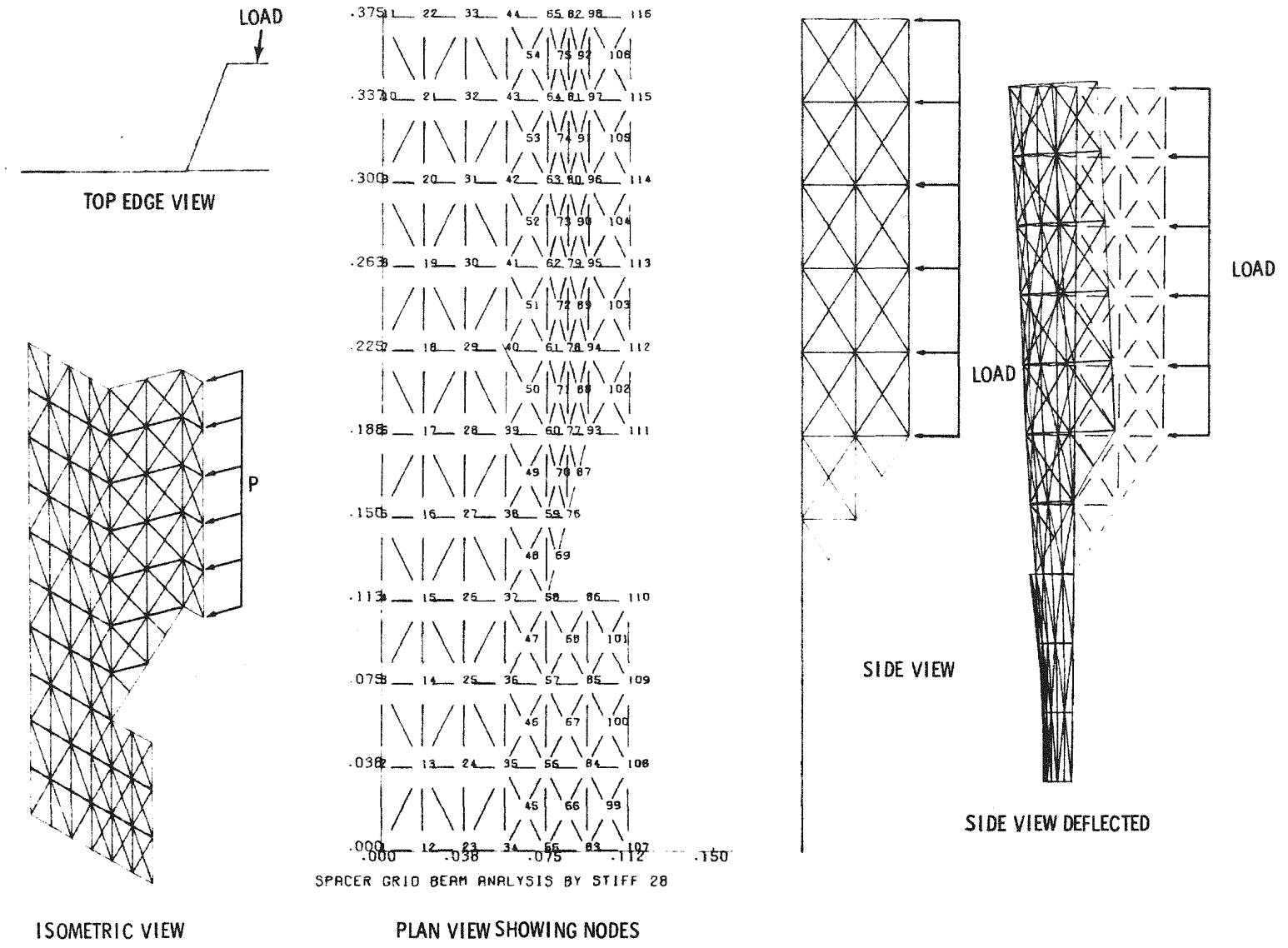

Fig. 3.10 Dimple model with tapered end

The actual deflections for the edge and center are shown in Fig. 3.11. The deflection of the plate centerline is shown in Fig. 3.12, which also shows the relative deflection of the dimple portion and web portion.

3.2.1.3. Spacer-grid Inplane Distortion. The accumulative effects of transverse rod loads on in-plane cell distortions are being investigated. The combined effects of all the fuel rods pushing in one direction can cause relatively large overall displacements compared to the motion of a single rod.

Preliminary work has shown that the peak-to-peak orientation appears to give the greatest distortions for a given rod load. The source of this type of loading is based on thermal bowing of the fuel rod and is limited to a maximum force of 1.0 lb/rod. This limit is based on the thermal gradients present in the rods and their inherent stiffness.

The model that is currently being used to investigate the interactions is shown in Fig. 3.13. It is composed of 320 nodes and 445 elements. The loading is applied to the model in the positive X direction. The magnitude of each local force vector is scaled to simulate a net 1.0 lb/rod load, and these load vectors are applied to simulate a uniform load condition. At present this work is still in progress; the effort is to develop an optimum set of boundary constraints that will accurately represent the actual conditions. Future work will include the effects of thermal distortions caused by thermal gradients across the spacer-grid assembly.

3.2.2. Thermal-hydraulic Analysis of Spacer-grid Mounting

The temperature of the duct wall of the fuel, blanket, and control assemblies depends on the coolant temperature and flow within the ducts, the insulating effect of the spacer-grid hanger straps located on the inner walls of the duct, the bypass flow of coolant around these hanger straps, and the recirculating flow outside the ducts resulting from the aspiration effect of the high-velocity coolant exiting from the ducts. During this quarter, the flow external to the fuel assemblies was evaluated and calculations of the distribution of bypass flow around the hanger straps were performed.

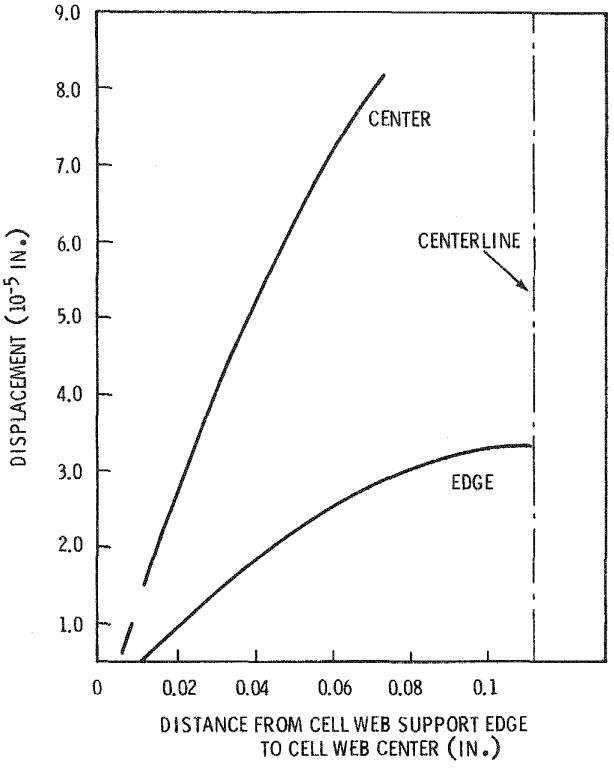

Fig. 3.11 Grid cell web distortion vs. position from support edge

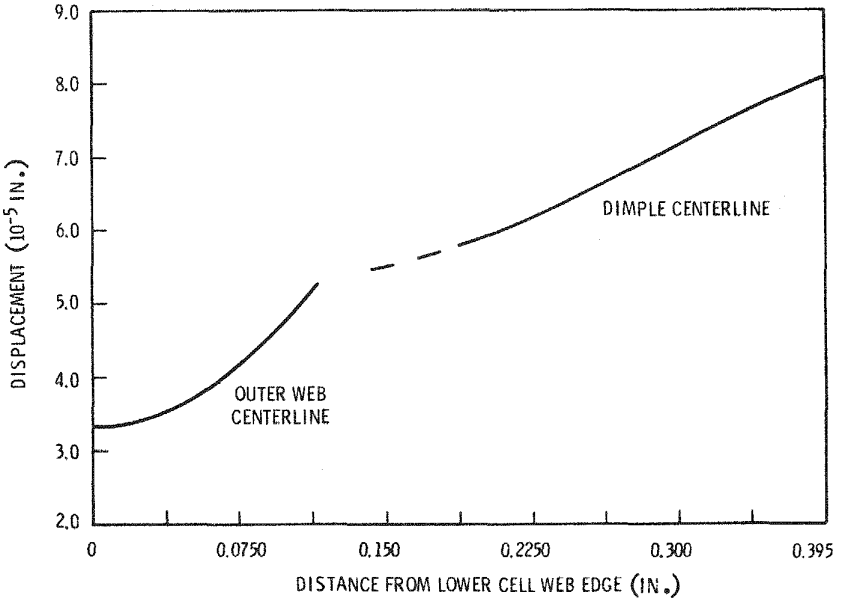

Fig. 3.12 Grid cell web centerline displacement vs. distance from outer edge to cell web center

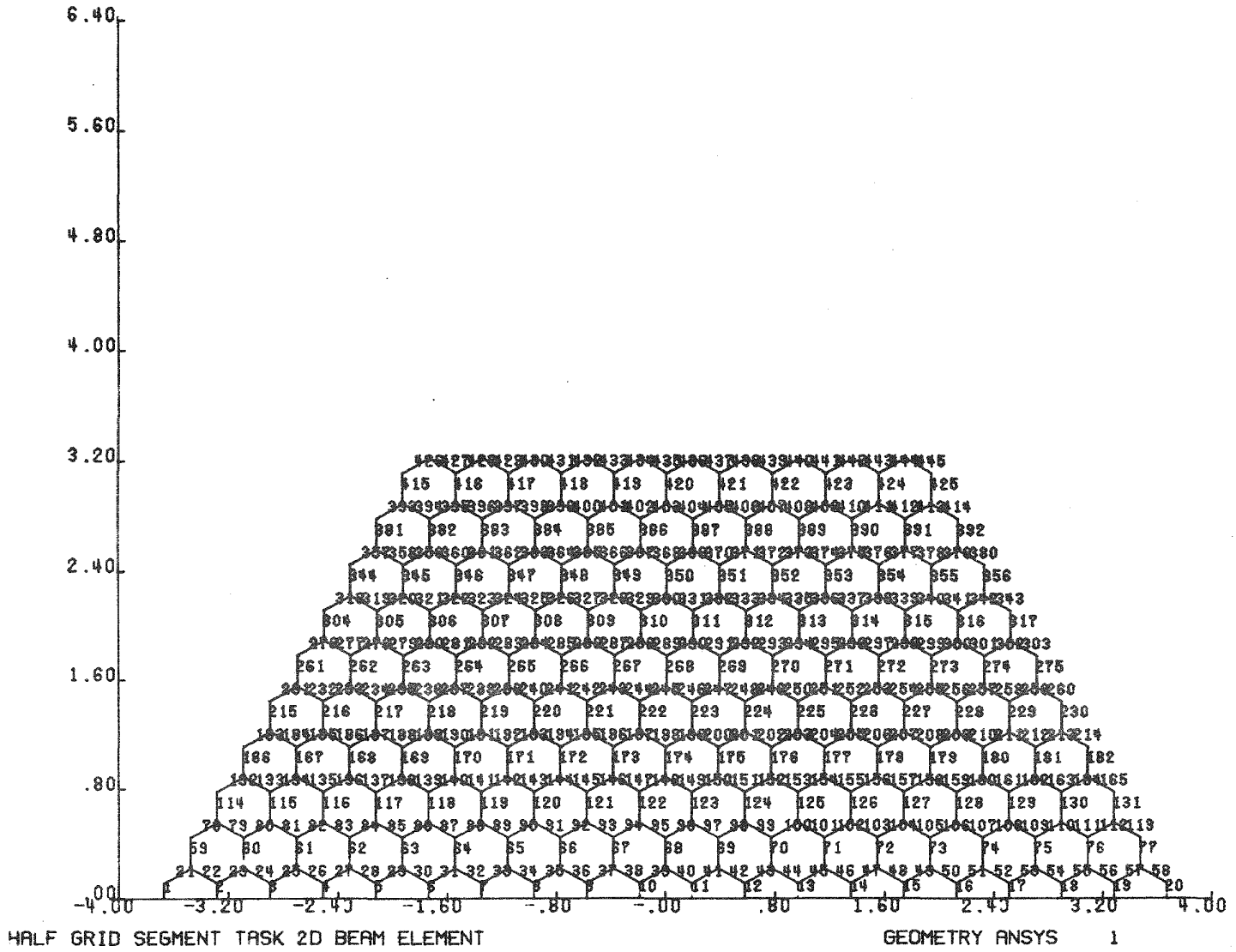

Fig. 3.13 Half-grid segment model using two-dimensional beam elements

3.2.2.1. Coolant Flow in Clearance Spaces Between Fuel, Blanket, and Control Assemblies. A calculation of the flow distribution in the clearance spaces between the fuel, blanket, and control assemblies has been performed using a network flow analysis code. Coolant flow between the fuel assemblies (inward radially and downward axially) results from the aspiration effect of the high-velocity coolant exiting the fuel ducts. The essential features of these calculations are:

1. At core outlet conditions of T = 1022°F and P = 1260 psia, the helium properties are: ρ = 0.312 lbm/ft^3, C_p = 1.2416 Btu/lbm-°F, μ = 0.095 lbm/ft-hr.

2. Spaces between fuel-element ducts were modeled as a grid of axial and radial flow paths. Azimuthal symmetry was assumed and a fuel-element spacing characteristic of the preirradiation core configuration was used, i.e., 0.25 in. below the top of the core and 0.15 in. above the core. Modeling of the narrower interelement spaces above the core indicated that these spaces had a small effect on the flow distribution and a negligible effect on the total recirculation flow.

3. Loss coefficients were applied to all radial flow paths to account for changes in the flow direction and cross-sectional flow area. Loss coefficients having values between 0.2 and 0.5 were used; the value used affected the flow distribution but had only a small effect on the total recirculation flow.

4. The driving pressure was calculated based on the dynamic head of the coolant exiting the fuel ducts. Expansion losses at the core outlet and the downstream dynamic head of the primary coolant flow were taken into account.

The results of these calculations are summarized in Figs. 3.14, 3.15, and 3.16. An R-Z schematic of the flow field in the clearance spaces between the fuel ducts is presented in Fig. 3.14. The axial downflow in the interelement channels as a function of radial position is plotted in Fig. 3.15 and the radial in-flow as a function of radial position is plotted in Fig. 3.16.

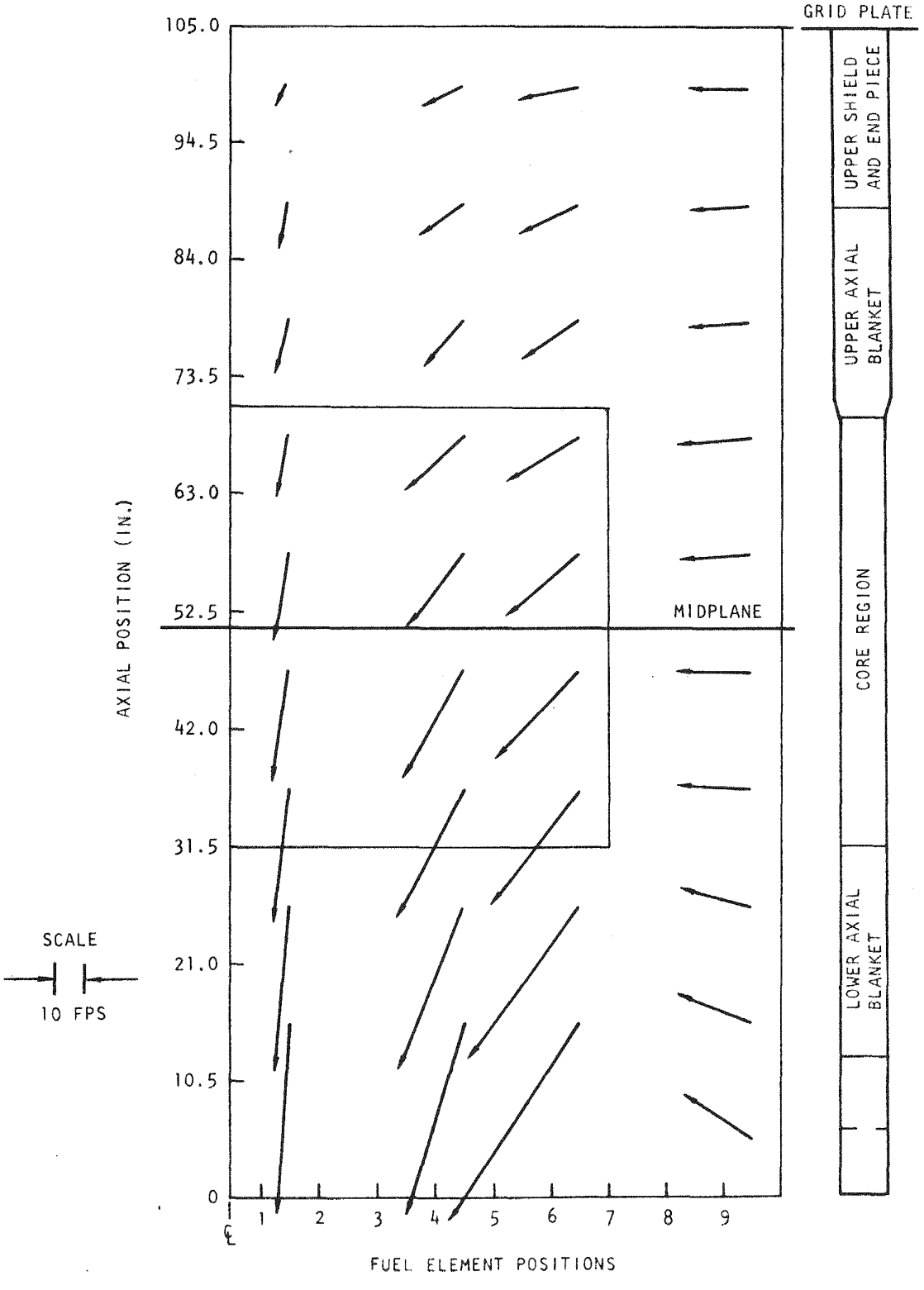

Fig. 3.14 R-Z flow field in channels between fuel ducts

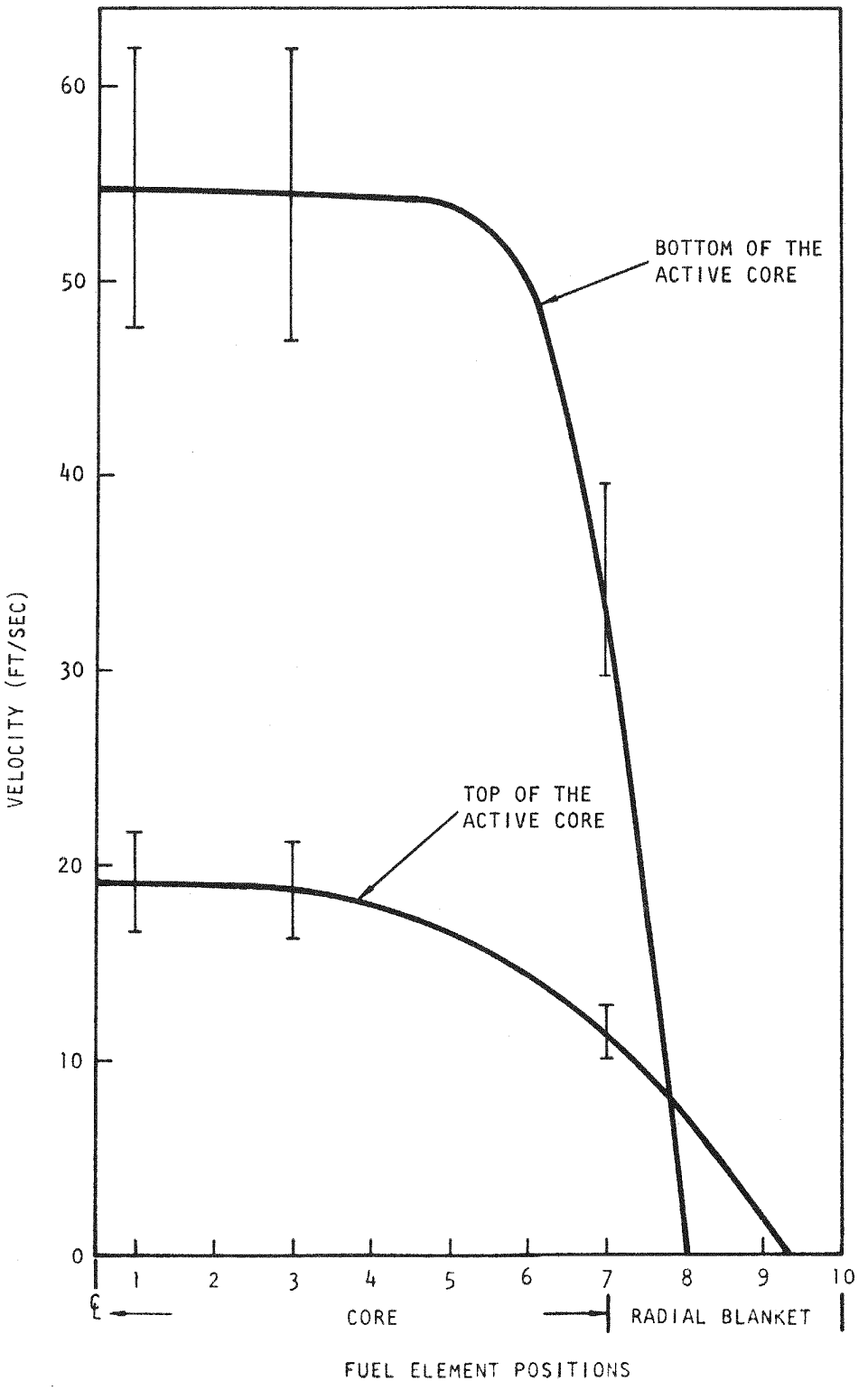

Fig. 3.15 Axial downflow component of flow between fuel ducts

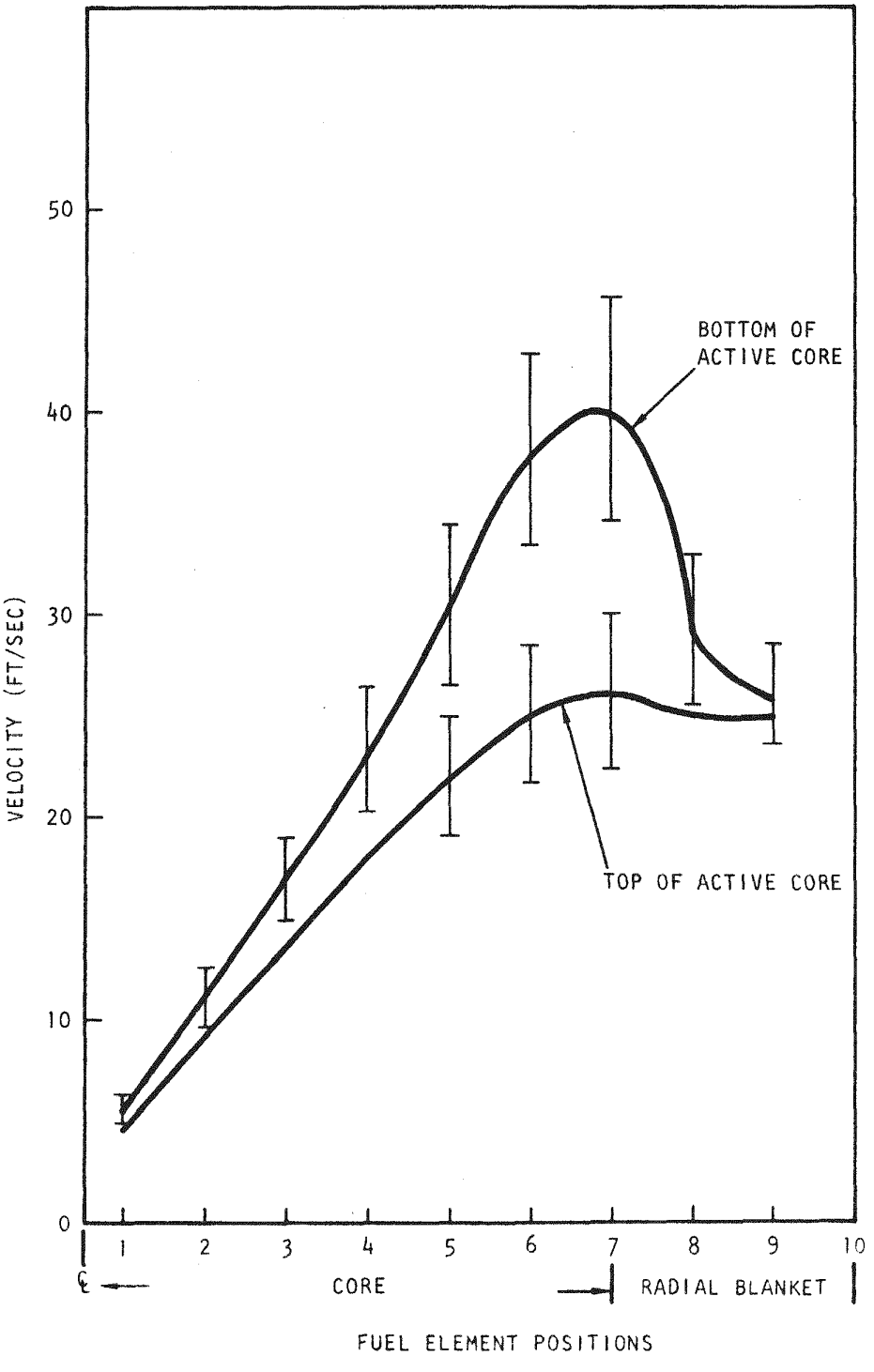

Fig. 3.16 Radial inflow component of flow between fuel ducts

The axial flow velocities are about 55 ft/sec at the bottom of the core and about half that value at the top of the core. The axial velocity distribution is relatively constant across the core and drops off sharply across the blanket. The radial velocities are 40 ft/sec at the outside blanket row and 20 ft/sec at the bottom and top of the core and reduce to near zero at the center of the core.

The driving pressure depends on the expansion losses downstream from the fuel assemblies. To account for the uncertainty in these losses, the results were calculated using variations in the driving pressure of 1.5 and 0.75, which brackets the uncertainties in the loss coefficient. The results of the uncertainty calculation are shown by the spread bars on Figs. 3.15 and 3.16. The resulting spread in velocities is small relative to the variations in driving pressure. This will result in a spread for the heat-transfer coefficients that will result from this flow velocity and will be taken into account for subsequent analysis of the duct temperatures.

3.2.2.2. Coolant Bypass behind Spacer-grid Hanger Straps. The spacer grids are supported from the duct wall by hanger straps, as shown on Fig. 3.17. These straps are slotted at the corners of the duct to allow for duct dilation to occur without directly loading the spacer grid. The grid hanger straps act as an insulation between the ducts and the main coolant flow because of the material in the hanger and the gas space between the hanger and the duct wall. The insulating effect of the gas space depends on the bypass leakage through the slots and down the fluted paths between the hanger and duct.

Analysis of the leakage flow and distribution through the slots in the spacer-grid hanger strap was performed using a two-dimensional network analysis that accounted for the difference in flow resistance in the transverse and axial directions between the fluted section of the hanger strap and the duct wall. The total flow bypass for the nominal geometry case is 0.68% of the total assembly flow. The bypass is removed with the coolant below each spacer grid. The flow through the first and second flute is 52% and 29% of the total bypass, respectively. The flow distribution from

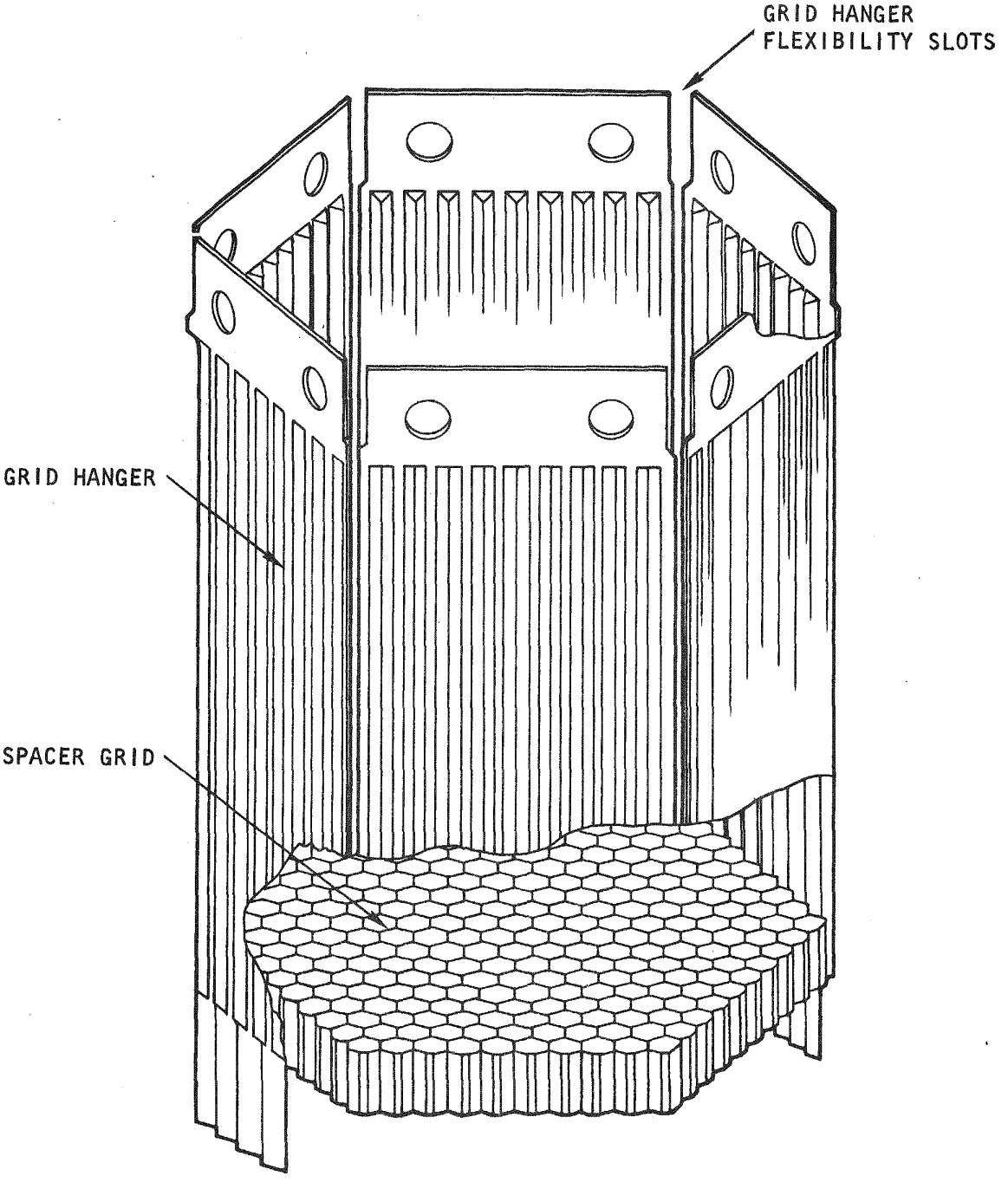

Fig. 3.17 Fuel-element spacer grid

this analysis can now be used to perform a temperature distribution analysis of the hanger strap and duct based on a more accurate evaluation of the effective conductance through the gap between the hanger and duct.

3.3. FUEL-ROD–SPACER INTERACTION TESTS

3.3.1. Test Program Objective

The objective of the rod-spacer interaction tests is to determine the range of H_2 and H_2O impurities in the GCFR helium coolant in which satisfactory performance of the spacer and fuel-rod interaction can be expected. The intermittent axial motion of the rod relative to the spacer could cause galling, adhesive wear, or metal-to-metal bonding. The contact of the rod and spacer during passive periods could lead to diffusion bonding. In addition, a significant amount of wear would reduce the wall thickness of the cladding tube and form a notch that could lead to a weakening of the cladding. The degree of these interactions may be controllable by the adjustment of the amount of H_2 or H_2O present in the helium.

The specific experimental objectives are to determine (1) the amount of wear, (2) the coefficient of friction, and (3) the appearance of wear or adhering surfaces as a function of impurity content, the normal force, temperature, number and length of the strokes, and the dwell time between strokes. The temperature range to be covered is 325°C to 750°C, which represents a range between the core inlet temperature to 50°C above the maximum hot-spot temperature. This higher temperature was selected to evaluate upper temperature limits for the rod-spacer interaction. Stroke lengths of 1.0-in. and 0.1-in. were selected as being representative of the two types of motion expected—namely, large, less-frequent excursions caused by small power changes. The dwell times between strokes are 1 hr for the 1.0-in. stroke test and 1-min for the 0.1-in. stroke test. These dwell times were chosen to provide the required number of strokes (100 and 4,000, respectively) to be accomplished in the test period of 100 hr. More recent analysis indicates that stroke lengths of 0.15 in. and 0.03 in. are more appropriate. All tests during this quarter were performed with a 0.15-in. stroke.

Various H_2O levels in the range of 90 μatm to 4,300 μatm are being used. Testing outside this range may be done if definite changes in behavior of

Table 3.1

RESULTS OF ROD-SPACER TESTS

Test No.[a]	Atmosphere (μatm)		Tube Type		Spacers		Number of Strokes	Total Linear Travel (in.)	Coefficient of Friction	
	H_2	H_2O	Alloy	Surface	Alloy	Type			Peak	Equilibrium
Spacers and Tubes for BR-2 Loop Tests										
15	30,000	300	316	Smooth	316	Pressed	100	15.0	1.4	1.0
16	30,000	300	4981	Smooth	4981	EDM	100	15.0	1.8	1.4
17	30,000	300	316	Smooth	4981	EDM	100	15.0	2.4	0.8
18	30,000	300	316	Ribbed	4981	EDM	100	15.0	1.5	1.1
19	30,000	300	4981	Ribbed	4981	EDM	99	14.9	1.0	0.6
20	30,000	300	4981	Smooth	4981	EDM	99	14.9	1.1	0.5
21[b]	30,000	300	4981	Ribbed	4981	EDM	98	14.7	n.d.	0.7
Type 316 SS EDM Spacer Test										
22	900	90	316	Ribbed	316	EDM	100	15	0.6	0.5
23	900	90	316	Smooth	316	EDM	100	15	0.8	0.6
24	900	90	316	Smooth	316	EDM	100	15	0.6	0.6
25	900	90	316	Ribbed	316	EDM	103	15.5	0.7	0.6
Inconel 718 Pressed Spacer Evaluation										
26	900	90	316	Smooth[c]	718	Pressed	52	7.8	0.4	0.1
Comparison of Etchant Influence[d]										
27	900	90	316	Smooth[e]	316	Pressed	27	4.1	1.0	---
28	900	90	316	Smooth[c]	316	Pressed	33	5.0	0.6	---
29	900	90	316	Smooth[e]	316	Pressed	57	8.6	0.4	---
5[f]	900	90	316	Smooth[e]	316	Pressed	6	6.0	1.7	---

[a] Tests 15, 16, and 17 were made at a gas flow rate of 50 cm^3/min; all of the remaining tests in this series were made at a gas flow rate of 100 cm^3/min.

[b] Test temperature 550°C.

[c] Ionetics etchant.

[d] Adhesion occurred in all of these tests.

[e] Powerkleen etchant.

[f] Stroke length 1.0 in. for this test only.

the rod-spacer interaction are not observed within that range. Hydrogen-to-water ratios in the range of 10 to 100 will also be evaluated.

Rod-spacer evaluations during this quarterly period consisted of tests of 20% cold-worked Type 316 and 1.4981 stainless-steel (SS) tubes versus 1.4981 electrodischarge-machined (EDM) spacers, Type 316 SS tubes versus Type 316 SS EDM spacers, a Type 316 SS tube versus an Inconel 718 spacer, and Type 316 SS tubes etched with two different etchant solutions. The method of surface-roughening the cladding tubes at GA to supply ribbed tubes for the rod-spacer interaction test has been changed from a solution with the trade name Powerkleen to a solution called Ionetics. The Ionetics solution produces a better shape and finish on the tube. A mechanical refrigerator has been installed to control more precisely the temperature of the water saturator when the test rig is running unattended.

The test results for the various tests conducted are given in Table 3.1.

3.3.2. BR-2 Loop Test Series

A series of seven tests (tests 15 through 21) were run on samples representative of fuel-rod and spacer components to be used in the 12-rod bundle in-pile loop test to be performed in the BR-2 reactor at Mol, Belgium. Spacers were fabricated by Kraftwerke Union (KWU) by electrodischarge machining 1.4981 stainless steel that was in the annealed condition. The hardness of the plate from which the spacers were cut is less than that of annealed Type 316 stainless steel. Tubing of 1.4981 alloy was supplied by KWU in two sizes, 0.236 and 0.295 in. (6.0 and 7.5 mm) OD and was 14% cold-worked. Tubing of the same lot as that used for the GA fuel rods for the experiment F-3, which is 20% cold-worked, was also used in this test series. Spacers for six tests were supplied. Test variables that were held constant are listed below:

Temperature	525°C (one test at 550°C)
Normal load	1.1 lb (0.5 kg) per spacer
Stroke length	0.15 in. (3.8 mm)
Dwell time	1 hr
H_2	30,000 μatm
H_2O	300 μatm
He	Balance

The test temperature in test 21 was increased 25°C to determine the effect of temperature on the oxidation characteristics of the test sample. The etchant solution was changed to Ionetics after test 16 and test 16 conditions were rerun as test 20 with the new solution. The smooth tubes were also etched in the solution so as to produce the same surface conditions as on the ribbed tubes. In addition, one test (test 15) was run in this test series atmosphere with a 316 SS tube and a 316 SS spacer that was pressed from a strip and spot-welded together. The test variables and measured results are given in Table 3.1. Adhesion did not occur in any of the tests and the coefficient of friction values are in the range previously observed. The equilibrium coefficient of friction is the average value from stroke 30 to 100.

Visual examination of the tubes at ∿30X shows generally light wear or only burnishing for the ribbed tubes, except for test 21 where one wear track was 0.03 in. wide at the top and up to 0.006 in. deep. The smooth tubes exhibited wear grooves that are difficult to measure but are estimated at less than 0.006 in. for test 16. Evidence of metal transfer was seen in the form of small nodules adjacent to the wear tracks. Detailed examination of the spacer contact surface will require sectioning; however, examination indicates little wear on the spacer except for one or more shallow grooves on several of the spacers. The surface appearance of the tubes is generally good, with no appearance of oxidation except at the wear sites. The one tube tested at 550°C had a dull appearance following the test. The spacers discolor and apparently undergo some surface oxidation.

Although these tests are limited in scope, several observations can be drawn from the results. Adhesion did not occur between smooth or ribbed tubes and the pressed or EDM spacers. The friction coefficients are too scattered to allow a correlation with tube surface condition or other parameters. The ribbed tubes exhibited less wear than the smooth tubes, except as noted for test 21.

3.3.3. EDM Spacer Test Series

The next series of tests was completed with Type 316 SS tubes versus EDM spacers fabricated by GA from a 20% cold-worked Type 316 stainless-steel bar. The spacers had flat contact surfaces with the tube samples

similar to the KWU spacers, but had a longer contact length of 0.375 in. (versus 0.29 in. for the KWU spacers) and rounded leading and trailing edges. The surface of the GA spacer is rougher (80 μin. AA versus 50 μin.) than the KWU spacer. The fixed test conditions were the same as for the previous tests. Other variables and results are listed in Table 3.1. The peak coefficient of friction is lower than in previous tests and the equilibrium coefficient of friction is at the low end of the range previously observed.

A significant point is that adhesion did not occur in this series at a H_2-to-H_2O ratio of 10 for a smooth tube. This adhesion had been observed in the initial test under similar conditions, as reported in the previous quarterly report.[1]

3.3.4. Evaluation of Inconel 718 Spacer

The next test (test 26) used a pressed Inconel 718 spacer against a Type 316 SS smooth tube to obtain a preliminary evaluation of the behavior of a dissimilar material. This test had a goal of 50 strokes. The test temperature was 525°C, other test variables and the results are given in Table 3.1.

Adhesion did not occur and the peak coefficient of friction (0.4) is the lowest observed to date.

3.3.5. Evaluation of Surface Etching Solution

Several tests were performed to determine the effect, if any, of the Powerkleen and Ionetics etchants on friction and wear behavior. One observation made previously was that tubes etched in Ionetics solution had a brighter surface appearance after testing. This indicated some difference in the surface that could influence friction behavior. The test conditions chosen were the same as for test 5, in which adhesion had occurred. The test temperature was 525°C. The test variables and results are shown in Table 3.1.

Adhesion occurred in each test and the total linear travel at the time of adhesion is in the same range. It is apparent from this test series that the two different etchants result in about the same friction and wear behavior.

REFERENCE

1. "Gas-Cooled Fast Breeder Reactor Quarterly Progress Report for the Period November 1, 1973 through January 31, 1974," USAEC, Report GA-A12894, General Atomic Company, April 12, 1974.

4. TASK 4120—FUEL- AND BLANKET-ELEMENT ASSEMBLIES

4.1. HEAT-TRANSFER AND FLUID-FLOW TEST

The planning for a helium-loop test series using electrically heated rods to simulate GCFR fuel-rod bundles is being carried out under this task. The development of the test facility, the Core Flow Test Facility (CFTF), and the execution of a test program are necessary to obtain information for the design of GCFR fuel, control, and blanket assemblies. The CFTF will be a 1,500-psia helium loop for testing the structural, thermal, and hydraulic characteristics of model GCFR assemblies under their initial design conditions and predicted end-of-life conditions, including simulated radiation-induced changes. The tests are to simulate the structural interactions that result from both steady-state and transient operational conditions and the effects of these interactions on the thermal-hydraulic performance are to be measured. These tests will provide experimental verification of the design analysis techniques for predicting the behavior of full-size GCFR assemblies. The work is being carried out under a joint program with the Oak Ridge National Laboratory (ORNL) in which GA is responsible for the test program and ORNL is responsible for the CFTF design.[1,2]

In the last quarterly period, an evaluation was made to establish the basis for the facility size in terms of power and flow requirements and range of test bundle sizes up to a maximum.[2] The evaluation recommended that the CFTF be designed for a capacity of 61 simulated core fuel rods with the expansion capability to 91 rods. During this quarterly period, at a meeting of the CFTF coordinating committee, the size evaluation was reviewed and a bundle size of 91 rods was adopted as a basis for loop design. The maximum full-power model sizes will be a 91-rod fuel assembly, a 90-rod control assembly and a full-size GCFR 127-rod blanket assembly.

Major emphasis at GA during the current quarterly period was centered on the preparation of a draft of the test program plan. An outline of the test plan was prepared that includes the objectives, the facility performance requirements, and the test-bundle size requirements, and divides the experimental program into a test series for each type of assembly:

1. Preliminary fuel-assembly models of relatively small size to check out facility performance and to determine if the fuel assembly design contains major design deficiencies.

2. Fuel-assembly models ranging in size up to the facility limit of 91 rods to verify experimentally all possible design predictions and to explore design and safety margins. Bundles consisting of 37, 61, and 91 rods will be tested to assure that predictive analysis correctly extrapolates from small-size bundles to larger-size bundles.

3. Control-assembly models of 54 and 90 rods to determine thermal-hydraulic performance and the interaction of the central control-guide tube with the surrounding rods and the spacer grid.

4. Blanket-assembly models of full-scale GCFR design to verify experimentally all possible design predictions, particularly the effects associated with large transverse power gradients.

5. Models of in-pile test assemblies to aid in assuring satisfactory in-pile operation and for comparing the results of out-of-pile tests with in-pile tests.

In addition, the phenomena and potential problem areas to be examined experimentally and the proposed application of the test data to the GCFR design and analysis will be presented in the program plan.

REFERENCES

1. "Gas-Cooled Fast Breeder Reactor Quarterly Progress Report for the Period August 1, 1973 through October 31, 1973," USAEC, Report GA-A12824, Gulf General Atomic Company, December 10, 1973.

2. "Gas-Cooled Fast Breeder Reactor Quarterly Progress Report for the Period November 1, 1973 through January 31, 1974," USAEC, Report GA-A12894, General Atomic Company, April 12, 1974.

5. TASK 4160—PRESSURE EQUALIZATION SYSTEM FOR FUEL

5.1. FUEL-ELEMENT AND VENT-CONNECTION-SEAL TEST PROGRAM

In the GCFR reference design, the fuel, control, and blanket elements and their vent connections are sealed to the grid plate by clamping the matching conical surfaces of the elements to the grid plate with a force sufficient to effect a seal and to support the elements, which are cantilevered from the grid plate. These element seals must function at the coolant-pressure difference between the reactor core inlet and exit plenums. The effectiveness of the seals over the life of the core is uncertain, not only because each element may be rotated or relocated several times over its useful life, but also because the seals must be effective in a high-purity, high-temperature helium environment while subject to mechanical, vibrational, and thermal effects. Most of the uncertainties are expected to be resolved in a two-part test program: (1) a materials screening test program for prevention of static adhesion of mated fuel-element and grid-plate parts and (2) leakage tests of fuel-element and vent-connection seals to the grid plate. Current progress in these activities is given below.

5.1.1. Static Adhesion Tests

The element-seal test program includes a simulation test of small-scale samples of conical seal parts clamped together and tested in a hot helium environment. The test will simulate the conditions of a full-scale fuel element clamped to a grid plate.

The procurement and assembly of the test apparatus and equipment is essentially complete. The test parts have been received and are shown in Fig. 5.1. However, inspection of dimensional tolerances and surface finishes indicates that rework of four pieces will be required. After the final machining has been completed, the test pieces will be weighed and macrophotographs will be taken of the conical seal surfaces.

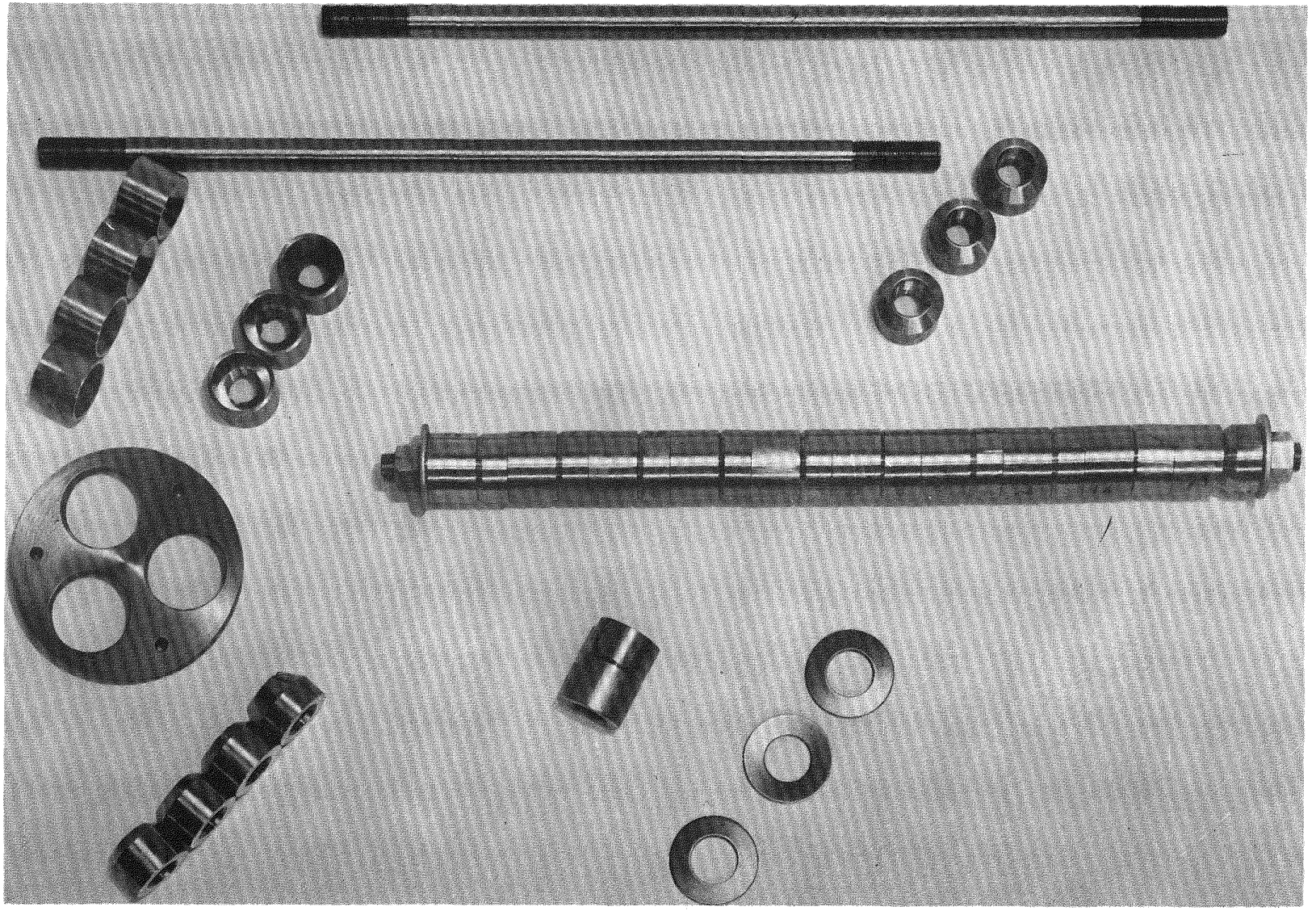

Fig. 5.1 Small-scale test parts for adhesion testing of fuel-element-to-grid-plate conical seal

The gas environment for the test has been established, at least for the initial tests, at 9,000 μatm of hydrogen partial pressure in the helium. This partial pressure will provide an H_2-to-H_2O ratio of 100, which has been found to be desirable on theoretical thermodynamics basis and from the fuel rod-spacer interaction tests (discussed in Section 3.3). Since the static adhesion tests will be conducted at 2 atm total gas pressure, six bottles of helium with 4,500 μatm or 4,500 ppm hydrogen content at 1 atm total pressure have been ordered as a source of gas for the tests.

The gas-environment control system is shown schematically in Fig. 5.2. The gas from the six storage bottles is metered at about 50 cm^3/sec and then filtered through a molecular sieve and charcoal trap. Moisture is added to the supply gas at the saturator upstream of the furnace and the H_2-to-H_2O ratio is measured downstream of the furnace. Moisture addition is increased or decreased at the saturator until the correct ratio is indicated by the ratio meter.

The moisture level in the environmental gas will be controlled to 90 μatm at the saturator. The water content of the gas will be established by the temperature of the water in the reservoir of the saturator. The water temperature is maintained by a refrigeration unit. All equipment items are on hand and ready to be installed in the system.

5.1.2. Seal Leakage Tests

Fabrication of the parts for the element and vent-connection-seal testing has continued. One set of stainless-steel forgings that simulate the conical seal parts of the grid plate and the fuel element has been fabricated and is being inspected. A photograph of these parts is shown in Fig. 5.3. The parts have a conical seal half-apex angle of 30° and a surface finish that has an average roughness of 16 μin. A second set of test parts is being machined by a different fabricator.

Design changes of the welding details had to be made to the pressure vessel of the test autoclave to be certified under Section VIII of the ASME Code. A detailed structural analysis was made for a design pressure of 75 psi at an operating temperature of 750°C to ensure its design adequacy. However, the vessel will meet the ASME Code requirements when it

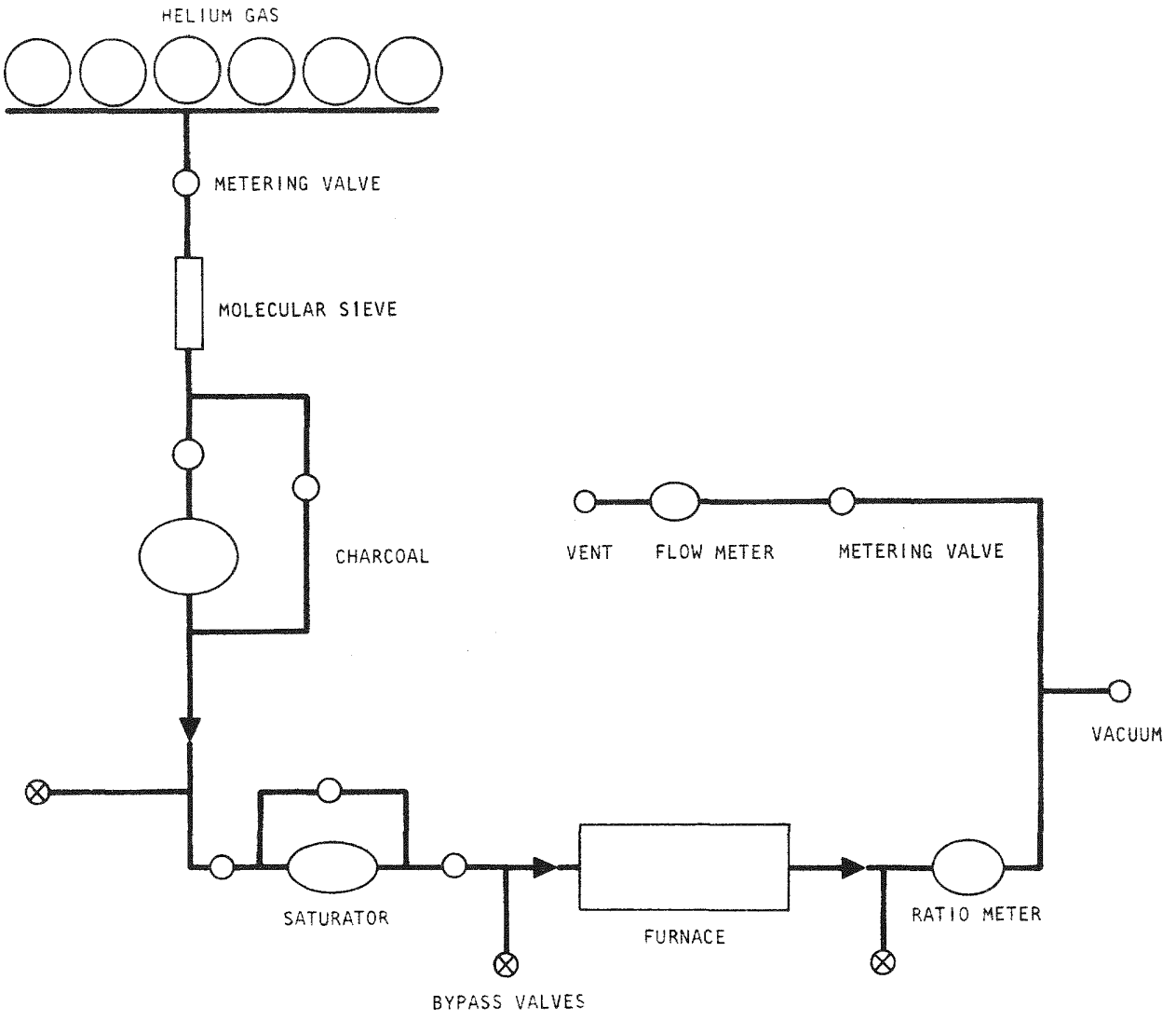

Fig. 5.2 Gas control and monitoring system for static adhesion test

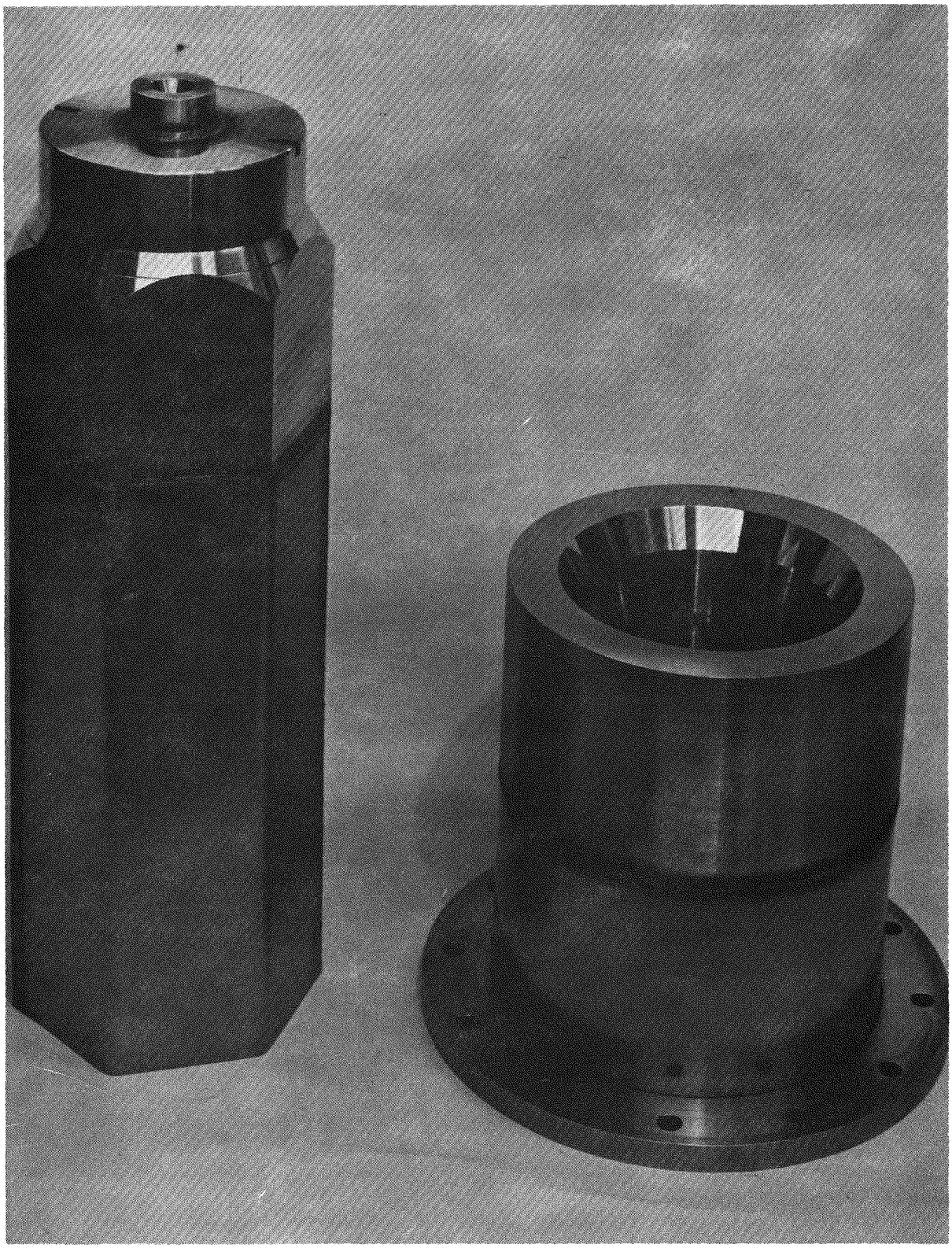

Fig. 5.3 Test parts for conical-seal leakage tests

is hydrostatically tested at 220 psi and room temperature. The materials and weld-joint designs have minimum safety factors of more than 3 relative to the seal-test operating conditions. The parts have not yet been received from the vendor because of the required design changes and the delays in procuring material.

The following test instrumentation has been received: (1) both load cells for load measurement, (2) Chromalox heaters for test temperature control, and (3) Conax feed-through glands and thermocouples.

5.2. MONITOR-SYSTEM ANALYSIS AND INSTRUMENTATION

Research and development are being carried out in this task to obtain design information for a system of stations and instrumentation to monitor the activity passing through the pressure equalization system from the fuel and blanket elements to the helium purification system. This monitoring system will measure activity signals resulting from leaks in the cladding of the rods in the fuel and blanket elements, but will reject activity signals arising from exhalation or depressurization. Correlations of signal patterns with the location of cladding leaks and with progressive changes in the conditions of the fuel and blanket elements will be developed.

Basic information on the isotopes (fission products) in the mixtures to be expected under leaking-element conditions will be measured by a Ge(Li) analyzer system that has been installed on the gas-sampling line of irradiation capsule GB-10, which has the unique capability of simulating a leak in an operating fuel rod in an element.

The Ge(Li) analyzer system has been designed with the aid of the computer program COUNT, which is being developed as a monitor-instrumentation design tool. Options for the Ge(Li) detectors and collimators have been written into the program. The COUNT program will subsequently be modified and then verified using the measured data obtained for various simulated leak conditions from the GB-10 irradiation experiment.

Mating of the Ge(Li) detector system with the counting chamber in the analyzer bypass in the sweep-gas sampling line was accomplished. However,

the final as-built separation distance of the detector from the counting chamber was 55.2 cm instead of the 38.1 cm previously expected. This required an adjustment of the collimator with the largest hole from a 1.27 cm radius (1 in. diam) to 1.59 cm radius (1.25 in. diam). The separation distance and collimator size changes resulted, according to the COUNT calculations, in essentially identical counting rates at all flow conditions as those previously calculated. Thus, the curves for count rate versus flow rate presented in Figs. 4.1 and 4.2 in the previous report[1] are applicable, with only a change in the separation distance (SEPD) and collimator size (RCOL).

Calibration of the series of five collimators ranging from 0.079 cm to 1.59 cm in radius was completed at ORNL; the data have not yet been received at GA for comparison with the COUNT computer code input and analyses. Scattering of low-energy gammas became pronounced with the 0.079-cm and 0.159-cm radii collimators.

Initial gamma spectra were taken on March 20, 1974, for the following flow modes, flow rates, and collimator sizes:

Flow Mode[a]	Flow Rate[b] (scc/min)	Collimator Diameter (in.)
TT-TT	800	1/2; 1-1/4
	160	1/2
BT-TT	250	3/16
BF-TT	160	3/16

[a] TT-TT - In and out through the top of the trap.
BT-TT - In through the bottom of the trap and out through the top of the trap.
BF-TT - In through the bottom of the fuel and out through the top of the trap.

[b] Irradiation capsule GB-10 was operating at 13.5 kW/ft and 200-psig helium pressure.

Computer analysis and data reduction of these gamma spectra are in progress at ORNL. The COUNT code calculations for the same analyzer conditions have been performed at GA for comparison with results. Simultaneously with the spectrum measurements, vial-bottle samples of the gases passing through the sampling line were taken by standard procedures established for the GB-10 irradiation capsule work. These samples will be analyzed in a laboratory Ge(Li) system for verification of the on-line analyzer results.

Analysis of the reduced Ge(Li) analyzer data for modifications and/or verification of the COUNT code will complete the design and installation of the on-line Ge(Li) analyzer. Routine operation of the Ge(Li) analyzer will be performed as a normal part of the irradiation capsule GB-10 subtask for the remainder of FY-74 and up to the end of the GB-10 capsule irradiation, which is expected to reach its burnup goal of 75,000 MWd/Te at the end of April 1975.

5.3. FUEL-ELEMENT FISSION-PRODUCT MANIFOLD

5.3.1. Screwed and Lock-ring Fuel-rod Connections to the Manifold

Leak tests have been performed to date on five of the six screwed and lock-ring connections being considered for attaching the fuel rods to the fission-product manifold:

1. Parker V,
2. Flat copper gasket (as fabricated and annealed),
3. Spark plug (matching conical surfaces, no gasket),
4. Flat bottom (a no-gasket type developed by KWU),
5. Mechanical lock-ring seals (see Fig. 5.4), and
6. Harrison K.

The first five types of connections were tested at room temperature and at ∿300°C. The results (see Table 5.1) indicate that the leakage for each type of seal (except for one sample of KWU No. 2) were several orders of magnitude below the specified maximum leak rate, even after breaking and remaking the seals three times. Outgassing of the Teflon seals at high temperature to determine the background (actual plus virtual) leakage has been found to mask the seal leakage. Soft malleable copper gaskets are now being used to replace the Teflon.

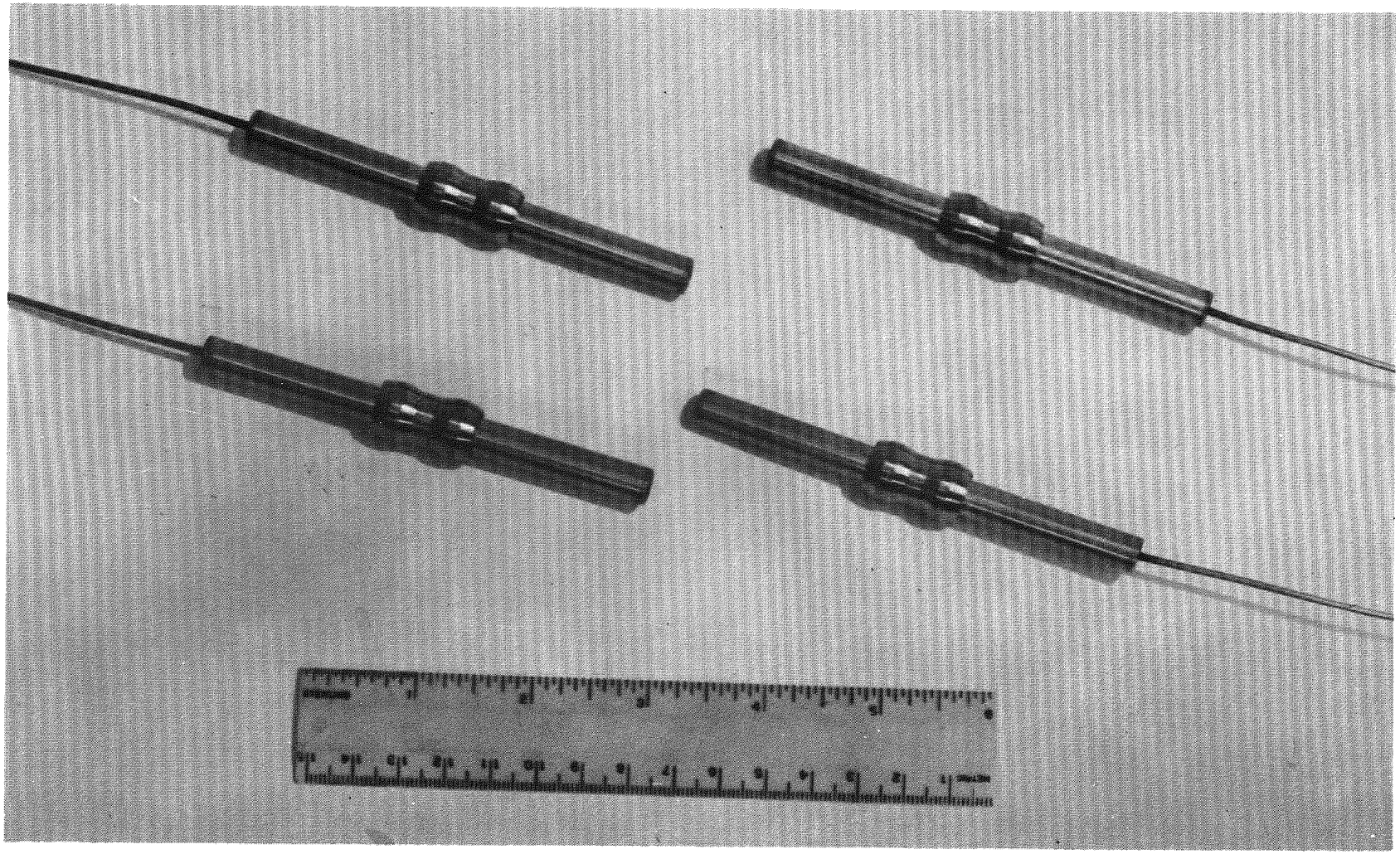

Fig. 5.4 Samples of lock-ring seal connections for fission-product manifold

Table 5.1

TEST RESULTS OF FUEL-ROD-TO-MANIFOLD CONNECTIONS

Temperature	Pressure (psig)	Vacuum (torr Hg)	Torque (in.-lb)	Sealing Finish (μin. RMS)	Type of Seal	Torr-liters per second
Ambient	Atm	2×10^{-5}	N/A	32	Teflon	1.77×10^{-7}
Ambient	Atm	2×10^{-5}	N/A	32	Teflon	1.08×10^{-7}
Ambient	Atm	2×10^{-5}	N/A	32	Teflon	1.12×10^{-7}
Ambient	Atm	2×10^{-5}	N/A	32	Teflon	1.18×10^{-7}
Ambient	29.4	3×10^{-4}	N/A	32	Parker V No. 1	1.44×10^{-7}
Ambient	29.4	3×10^{-5}	N/A		Parker V No. 1	5.77×10^{-7}
Ambient	29.4	3×10^{-5}	N/A		Parker V No. 1	2.93×10^{-7}
Ambient	29.4	3×10^{-5}	N/A		Parker V No. 1	3.30×10^{-7}
Ambient	Atm	3×10^{-5}	N/A	34	Teflon	1.62×10^{-6}
Ambient	Atm	2.5×10^{-5}	N/A	34	Teflon	1.19×10^{-6}
298°C	29.4	1×10^{-4}	N/A	34	Parker V No. 2	1.73×10^{-5}
294°C	29.4	1×10^{-4}	N/A	34	Parker V No. 2	2.08×10^{-5}
310°C	29.5		N/A	34	Parker V No. 2	1.31×10^{-5}
Ambient	Atm	1×10^{-5}	20	16	Teflon	1.4×10^{-6}
Ambient	Atm	2.8×10^{-4}	20	16	Unannealed Cu	3.27×10^{-6}
Ambient	29.5	3.6×10^{-5}	12	32	Annealed Cu No. 1	4.03×10^{-6}
Ambient	29.5	2×10^{-5}	13	32	Annealed Cu No. 1	1.5×10^{-6}
Ambient	29.5	7×10^{-6}	14	32	Annealed Cu No. 1	5.69×10^{-7}
305°C	29.5	7×10^{-6}	12	32	Annealed Cu No. 2	1.52×10^{-6}
296°C	29.5	8×10^{-6}	13	32	Annealed Cu No. 2	8.0×10^{-7}
300°C	29.5	8×10^{-6}	14	32	Annealed Cu No. 2	7.08×10^{-7}
Ambient	Atm	3×10^{-5}	10	32	Teflon	1.43×10^{-6}
Ambient	29.5	3×10^{-5}	10	32	Teflon	1.4×10^{-6}
Ambient	29.5	7.2×10^{-6}	40	40	Spark-plug cone	6.59×10^{-7}
Ambient	29.5	8×10^{-6}	45	40	Spark-plug cone	6.78×10^{-7}

Table 5.1 (continued)

Temperature	Pressure (psig)	Vacuum (torr Hg)	Torque (in.-lb)	Sealing Finish (μin. RMS)	Type of Seal	Torr-liters per second
Ambient	29.5	$1x10^{-5}$	50	40	Spark-plug cone	$1.44x10^{-6}$
Ambient	29.5	$3x10^{-5}$	40	Could not be measured	KWU No. 1	$9.99x10^{-6}$
Ambient	29.5	$1x10^{-5}$	45	Could not be measured	KWU No. 1	$1.4x10^{-6}$
Ambient	29.5	$8x10^{-6}$	50	Could not be measured	KWU No. 1	$9.03x10^{-7}$
Ambient	29.5	$8x10^{-6}$	52	Could not be measured	KWU No. 1	$6.97x10^{-7}$
293°C	29.5	$1x10^{-5}$	45	Could not be measured	KWU No. 2	$1.14x10^{-6}$
298°C	29.5	$7x10^{-5}$	47	Could not be measured	KWU No. 2	$9.12x10^{-6}$
Ambient	29.5	Would not seal	50	Could not be measured	KWU No. 2	Would not seal
302°C	29.5	$1.4x10^{-5}$	4	40	Spark-plug cone	$8.29x10^{-7}$
298°C	29.5	$5.4x10^{-5}$	90	40	Spark-plug cone	$6.42x10^{-6}$
296°C	29.5	$2.4x10^{-5}$	100	40	Spark-plug cone	$3.45x10^{-6}$
Ambient	29.5	$1x10^{-4}$	N/A	N/A	Lock ring	$4.44x10^{-7}$
310°C	29.5	$1x10^{-4}$	N/A	N/A	Lock ring	$2.98x10^{-6}$

[a]Teflon seals are used in place of test seals to allow measurement of the actual or virtual leak rate of the testing apparatus. Teflon has now been replaced with soft copper because of excessive outgassing at elevated temperatures.

The lock-ring seals were also leak-checked on a helium mass spectrometer at room temperature and were found to be leaktight within the limits ($<1 \times 10^{-9}$ cm^3/sec) of the mass spectrometers, indicating that the leak-rate measurements with the test rig are measuring entrapped gas within the seal itself, rather than the actual leak across the seal.

5.3.2. Alternative Design Evaluation

Four alternative designs of the manifold will be evaluated for amenability to fabrication and inspection. A compilation of source information previously obtained, such as vendor quotations and comments on process advantages and disadvantages, for the evaluation is being assembled. Cost quotations from the Component Manufacturing Department at GA have been received on the support grid and plenum design and on the reference design single-level manifold with screwed connections. Requests for quotations and comments have also been sent to the GA Component Manufacturing Department and several vendors for a two-level variation of the reference design and for a fourth design similar to the reference design except that the rods are connected to the manifold by welding through holes in the top of the manifold. The open holes are subsequently closed by welding on a cover plate shaped to match the manifold structure.

The four alternative manifold designs are currently being evaluated for fabricability, inspectability, and cost. When the current evaluation is completed, the designs will be evaluated for their reliability and adaptability to assembly in the fuel element (and the effect on element assembly sequence and inspectability).

The approach being employed to perform the evaluation of the four manifold designs consists of

1. Fabricating small segments of the manifold design to identify fabrication problems, to establish feasibility, and to determine some measure of the cost and inspectability of the concepts. For instance,
    a. A hole (0.05 in.) was drilled by the EDM method through a representative length (6-1/4 in.) of a web of the reference

manifold. Inspection results showed that the hole can, in fact, be produced with the hole diameter and runout over its length to the specified tolerances (0.005 in.)

b. A sample of a manifold that is a variation of the reference design with a grooved and welded cap (so that no hole drilling is required) is being made to demonstrate fabricability.

2. The GA Component Manufacturing Department is preparing comments on the methods of fabrication and inspection that can be employed, the fabricability and inspectability, and the relative cost for each of the concepts. It is anticipated that four methods of fabrication—EDM, ECM, investment casing, and conventional machining—will be evaluated. Preliminary evaluations to date are as follows:

   a. The reference design appears to be the most costly of the designs because more tooling and labor is required for its fabrication. The reliability and adaptability to element assembly have to be evaluated.

   b. The support-grid and plenum design is probably the least costly to fabricate because the tooling is the simplest and the least machining and inspection are required. Reliability and adaptability to element assembly have to be evaluated.

Based on these evaluations, the cost of the two-level design is expected to be equivalent to that of the reference design. Comments on fabricability and inspectability should be received early next month.

An evaluation of the welded-cap design with respect to cost, fabricability, and inspectability will probably be intermediate between 1 and 2, above. The welded-cap design has one obvious merit in that the fuel rods can be handled in the sealed condition at all times prior to installation of the cap for the manifold. The seals can be opened, by drilling or some other method, and visually inspected to ensure that the rods are vented prior to installation of the cap. This procedure is not possible with the other three designs.

These preliminary conclusions may be changed when additional information has been received from other fabricators.

REFERENCE

1. "Gas-Cooled Fast Breeder Reactor Quarterly Progress Report for the Period November 1, 1973 through January 31, 1974," USAEC, Report GA-A12894, General Atomic Company, April 12, 1974.

6. TASK 4170—THERMAL SHIELDING

The reactor thermal shield for the GCFR will protect the prestressed concrete reactor vessel (PCRV), the core support system, and other components from excessive radiation-induced effects, such as heating and degradation of materials. The development program for the GCFR thermal shield will include analytical and experimental tasks to establish the integrity and performance of the shielding materials under anticipated operating conditions for the life of the PCRV and core support structures. The shielding experimental program will verify performance predictions of radiation attenuation, internal heat generation, heat-removal capabilities, and longevity and integrity of the proposed shielding materials.

The initial effort on this task is to review and update the shielding development program plan presented in the overall development program plan for the GCFR demonstration plant,[1] to evaluate the shielding test requirements, and to coordinate planning for a test program with ORNL.

The initial physics analysis of the shielding included the generation of neutron and gamma-ray cross sections and a preliminary 10-group S_N calculation of the radial shield configuration.

A series of GGC-5 calculations were made using ENDF/B Version III libraries to obtain neutron multigroup cross sections averaged over the appropriate spectrum for the core, blanket, shield, and PCRV regions. A 10-group set and 24-group set were generated. The gamma-production cross sections were generated with the LAPHN code developed at LASL. This code reads ENDF/B data tapes and generates multigroup neutron-to-gamma-ray transfer cross sections. The gamma-ray transport cross sections were generated with the GAMLEG code.

These three phases will be combined, as shown in Fig. 6.1, to produce a coupled neutron-gamma-ray cross-section library.

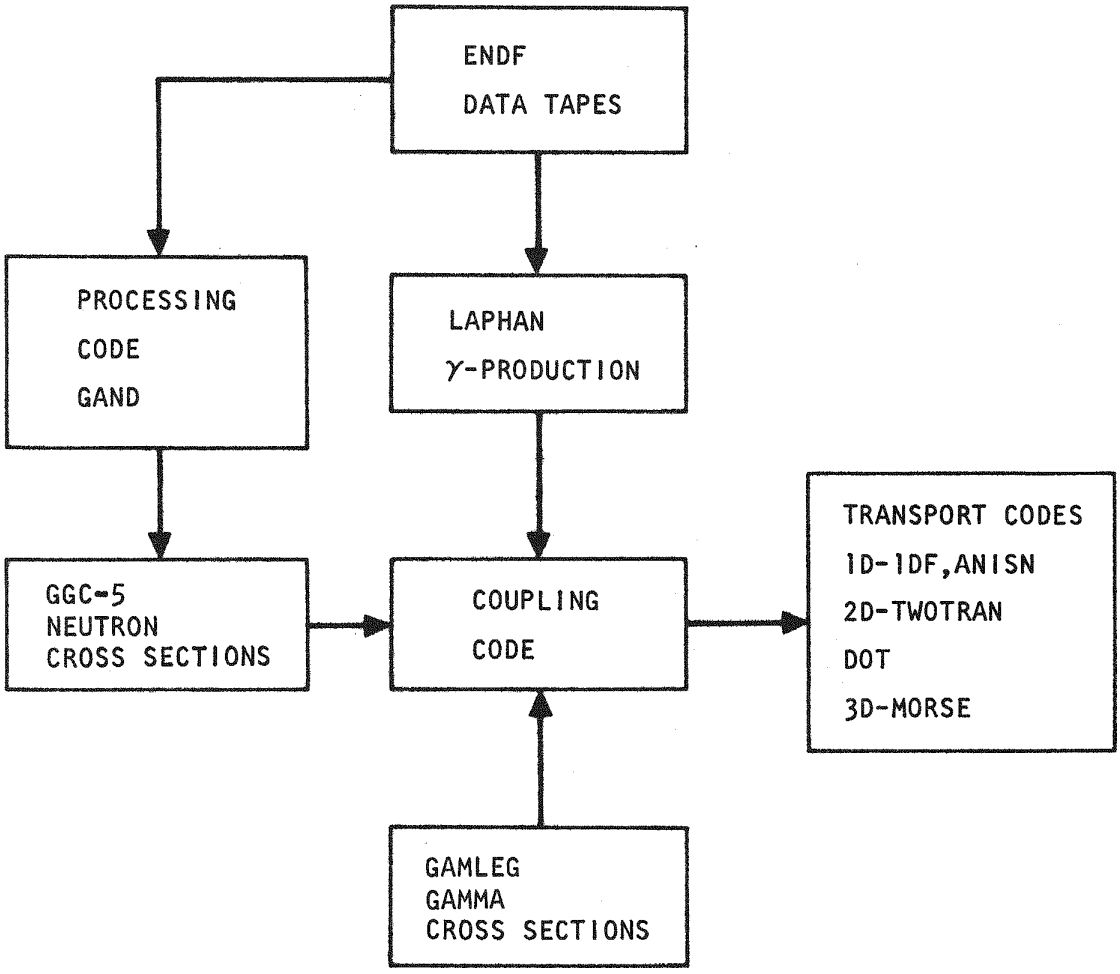

Fig. 6.1 Flow diagram for shielding calculations

A preliminary 10-group S_6-P_3 calculation was made for the shield configuration shown in Fig. 6.2. The design criteria for the radial shield are:

1. The total fast fluence (E > 1.0 MeV) at the liner shall not exceed 2×10^{18} nvt over the life of the liner (normally 40 yr).
2. The total nuclear heating rate in the PCRV shall not exceed 1 milliwatt/cm^3.
3. The lifetime dose to the tendons shall not exceed 5×10^8 rads.

The corresponding fluxes for the above criteria are:

$$\phi_{fast} < 2 \times 10^9 \text{ n/cm}^2\text{sec}$$

$$\phi_{thermal} < 1 \times 10^9 \text{ n/cm}^2\text{sec}.$$

The results for the radial shield calculations for the geometry shown in Fig. 6.2 are given in Fig. 6.3. These indicate that the present shield configuration is overly conservative for the fast-flux requirement and that it adequately meets the heating-rate criterion for the PCRV. These results will be compared with similar calculations performed at ORNL.

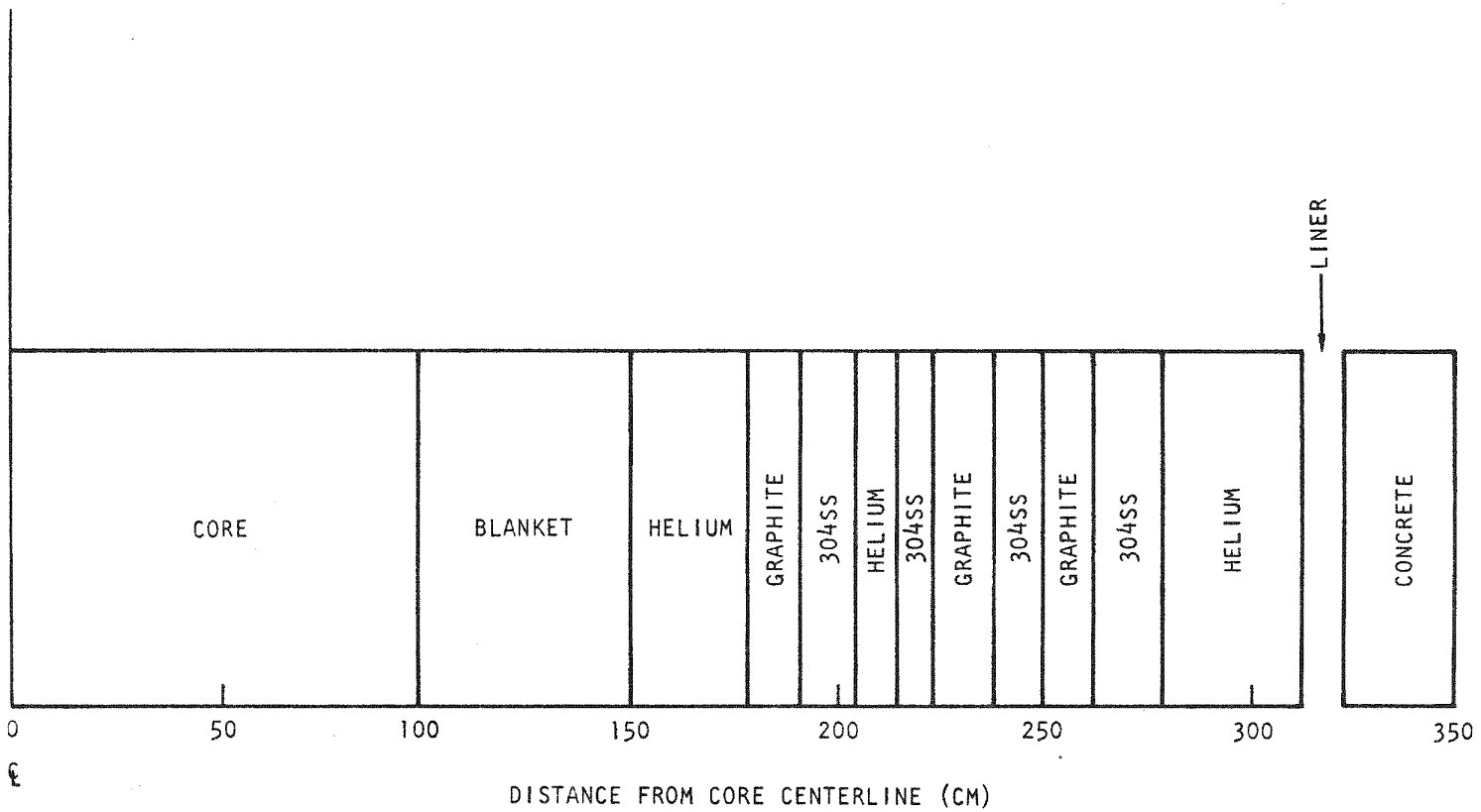

Fig. 6.2 Geometry for 1-D transport calculations

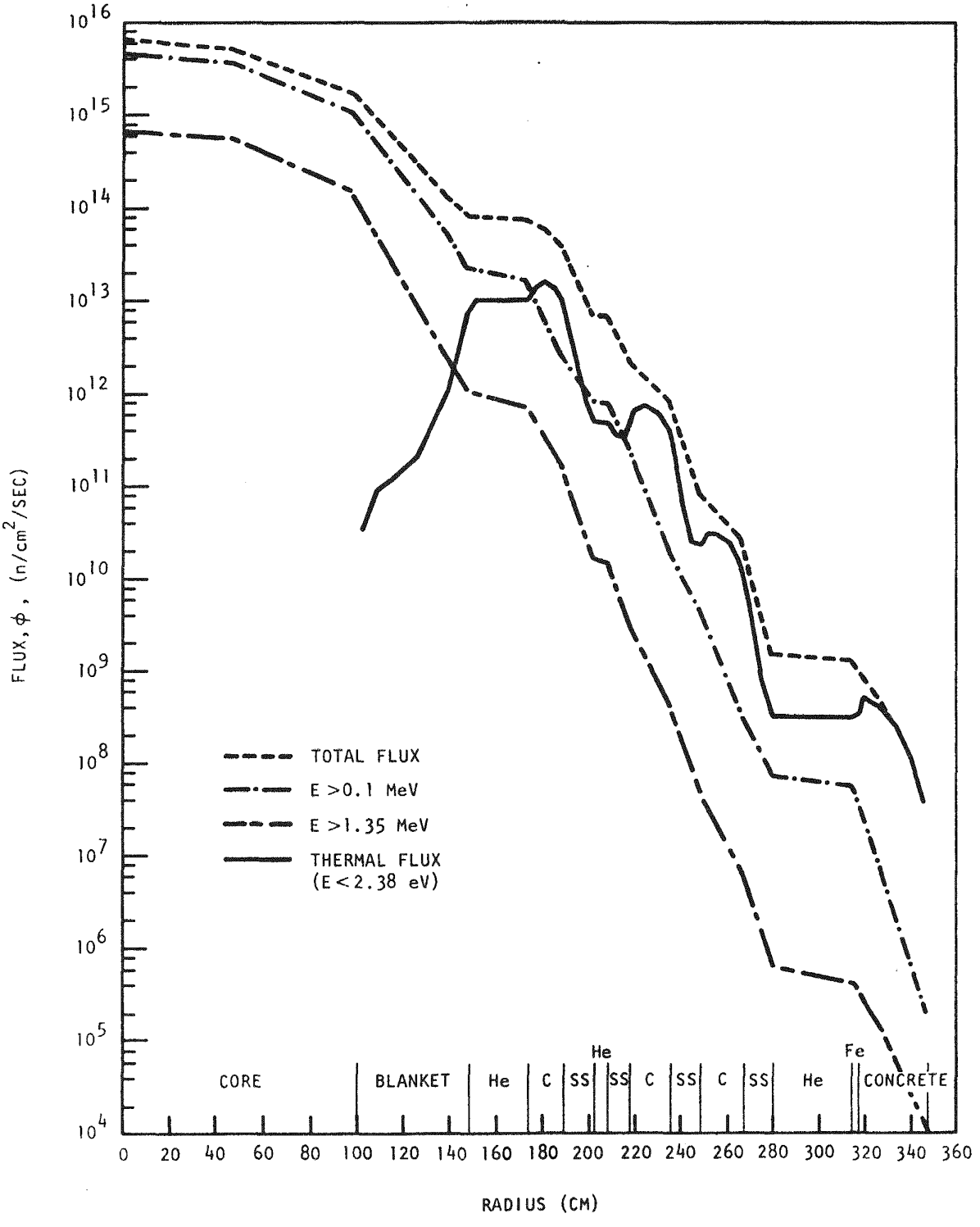

Fig. 6.3 Radial flux profile at the core midplane

7. TASK 4200/4400—FUELS AND MATERIALS DEVELOPMENT

7.1. THERMAL-FLUX IRRADIATION EXPERIMENTS

7.1.1. Irradiation Capsule GB-9

All laboratory analyses of the charcoal trap from irradiation capsule GB-9 have been completed and were reported in the previous quarterly report.[1] During the present quarter, some analyses of the results of the isotopic cesium contents of the trap have been carried out with the objective of elucidating the transport mechanism or transporting species.

An outline has been developed for the summary report on the postirradiation examination of capsule GB-9.

7.1.2. Irradiation Capsule GB-10

The sweep-gas vented-fuel-rod capsule GB-10 has achieved a burnup of 43,000 MWd/Te of the exposure goal of 75,000 MWd/Te. Of the exposure to date, 27,000 MWd/Te was accumulated at 12 kW/ft (565°C cladding outside temperature) and 16,000 MWd/Te was at 13.5 kW/ft (630°C cladding outside temperature).

Studies of the effect of pressure level on the active fission-product gases released from the GB-10 fuel rod continued. Capsule GB-10 was operated at a low-pressure level (200 psi versus the normal 1000 psi) for an exposure period of ∿5,000 MWd/Te, when the ORR was shut down for scheduled refueling and maintenance. During operation of GB-10 at 200 psi, four sets of gas samples were taken for analysis.

After startup of the ORR following the shutdown in March, capsule GB-10 continued operation at 13.5 kW/ft (630°C cladding temperature) but at 300 psi helium pressure. Operation at this third pressure level will be maintained for an exposure of ∿5,000 MWd/Te, which will complete the pressure-level tests. Power-cycling and depressurization testing will be carried out prior to increasing the power to 14.8 kW/ft (at a cladding

outside temperature of 685°C). Sampling of the fuel region of the GB-10 rod may be prohibited at this higher power level because of the high radiation levels in the sampling system.

Planning for tritium monitoring in capsule GB-10 has been initiated and a schematic of the instrumentation was developed. The system, as presently conceived, will utilize a liquid-nitrogen-cooled charcoal trap to effect the primary separation of tritium from the fission gases that are retained on the charcoal. This type of system is operating in the Peach Bottom Atomic Power Station and a similar system has been installed in the Fort St. Vrain Nuclear Generating Station. However, provision will also be made for the addition of a palladium-silver alloy diffusion membrane for further separation of tritium and the fission gases if the charcoal trap should prove inadequate.

The major instruments are available at GA. A test and calibration apparatus will be constructed to ensure that the proposed monitoring system will perform as expected. The system will be tested using tritium tracers in helium and helium tagged with Kr^{85} to simulate fission gases.

7.2. FAST-FLUX IRRADIATION EXPERIMENTS

7.2.1. Fast-flux Irradiation Experiment F-1 (X094B)

The irradiation of the seven-fuel-rod capsule F-1 (X094B) experiment has continued in EBR-II, and maximum burnup exposures up to 70,000 MWd/Te were achieved up to the time the EBR-II was shut down on April 9, 1974, for annual maintenance (which lasts approximately eight weeks). When EBR-II operation is restarted, irradiation of the F-1 subassembly will continue to a burnup of 75,000 MWd/Te on the remaining initial fuel rod (G-4), at which point a third and final interim examination is planned. The maximum burnup goal for the experiment is 100,000 MWd/Te.

The examination of the five rods (G-1, G-2, G-5, G-6, and G-7) removed from the F-1 experiment during the second interim examination (at 50,000 MWd/Te) is continuing at ANL. Examination of the G-1 fuel rod, which had operated at a cladding temperature of ∿800°C for a peak burnup of ∿56,000 MWd/Te, indicates that the diametral strain was no more than 0.3% (see Fig. 7.1) and that the cladding attack was no more than 2.5 mils in depth.

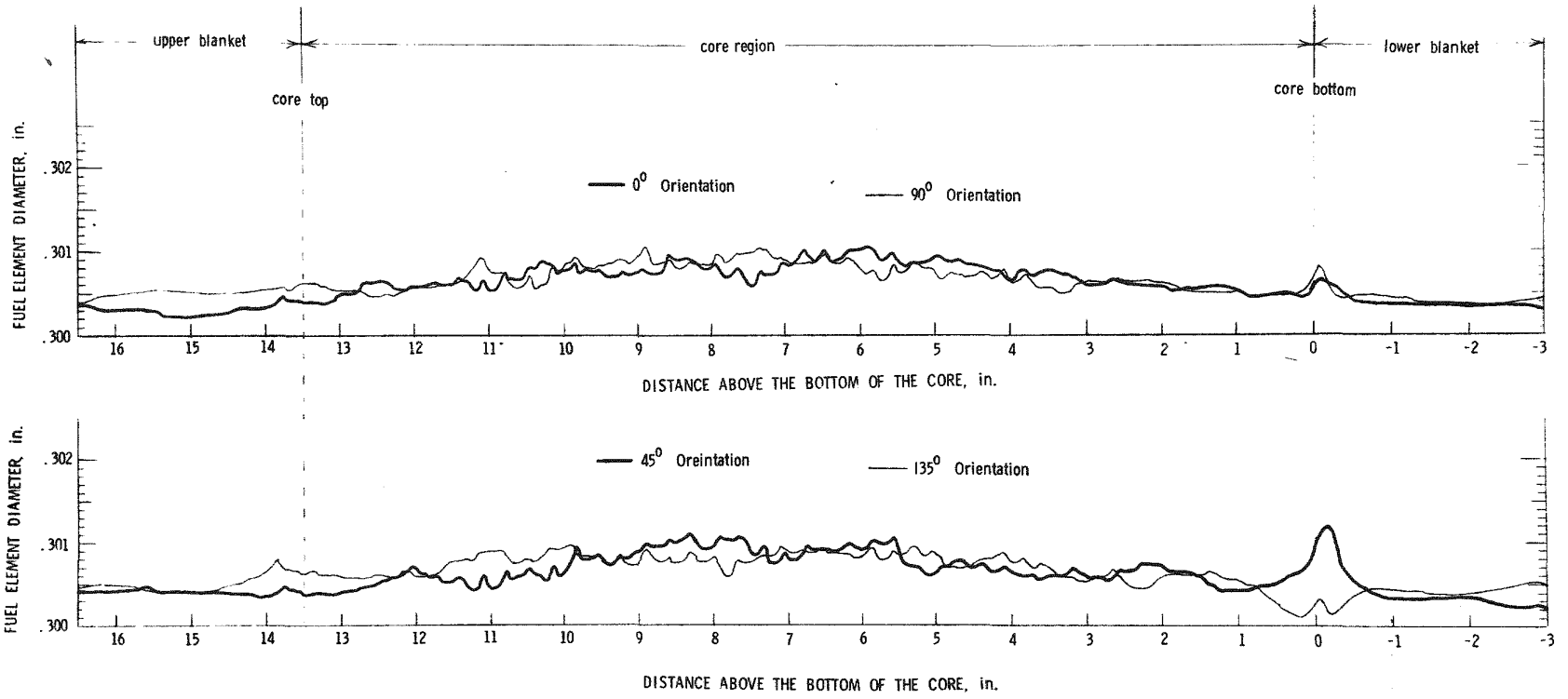

ANL-MSD-168570

Fig. 7.1 Postirradiation diameter measurements (profilometry) of fuel rod G-1, which operated at a maximum rating of 16.1 kW/ft and a maximum cladding temperature of ~800°C to a peak exposure of 56,000 MWd/Te (maximum diameter change = 0.8 mil; maximum $\Delta D/D_0$ = 0.27%)

This attack occurred in regions between and not adjacent to, cracks in the fuel periphery (see Figs. 7.2 and 7.3). This phenomenon has not been observed or reported in the literature nor is an explanation currently available. The presence of fuel melting was observed at the center of the rod (see Fig. 7.4). A porous region exists in the outer periphery of the columnar grains and the equiaxed grain-growth region appears very dense and extends to within a few mils of the cladding (see Fig. 7.5). Fuel migration by vapor transport resulted in closure of the central hole in the annular pellets at the end of the fuel columns near the upper and lower fuel-blanket interfaces (see Figs. 7.4 and 7.6), as seen previously.[2] The measured gas flow rate through the interior of the rod at the fuel-blanket interface is a factor of 10 lower than in previously examined irradiated fuel rods G-1 and G-3. This lower flow rate is thought to be associated with the large amount of volatile fission-product (cesium) migration to the fuel-blanket interface (see Fig. 7.7).

An analytical study of the gamma-scanning data obtained during the second interim examination of the F-1 (X094A) subassembly has continued at GA. During the quarter, attempts were made to quantify the results on the migration of volatile fission products that had been reported qualitatively in previous reports.[3]

The study of fission-product transport in the F-1 fuel rods has concentrated on four nuclides, which are easy to detect and whose behavior typifies that of other fission products. These are the nonvolative (refractory) Zr^{95}, the volatile species Cs^{137} and I^{131}, and Ba^{140}/La^{140}, which has both a gaseous (but very short-lived) and a volatile precursor.

For a stable species such as Zr^{95}, the axial profile shows a sharp drop in activity at the fuel-blanket interface. For volatile species such as iodine or cesium, enhanced concentrations are found at the fuel-blanket interfaces and some further migration into the blanket region was observed. Activity peaks of a smaller magnitude (but still indicating enhanced concentrations) were also found for the mass-140 chain. The transport of Cs^{140} over short distances was postulated to explain the observation of Ba^{140}/La^{140} concentrations.

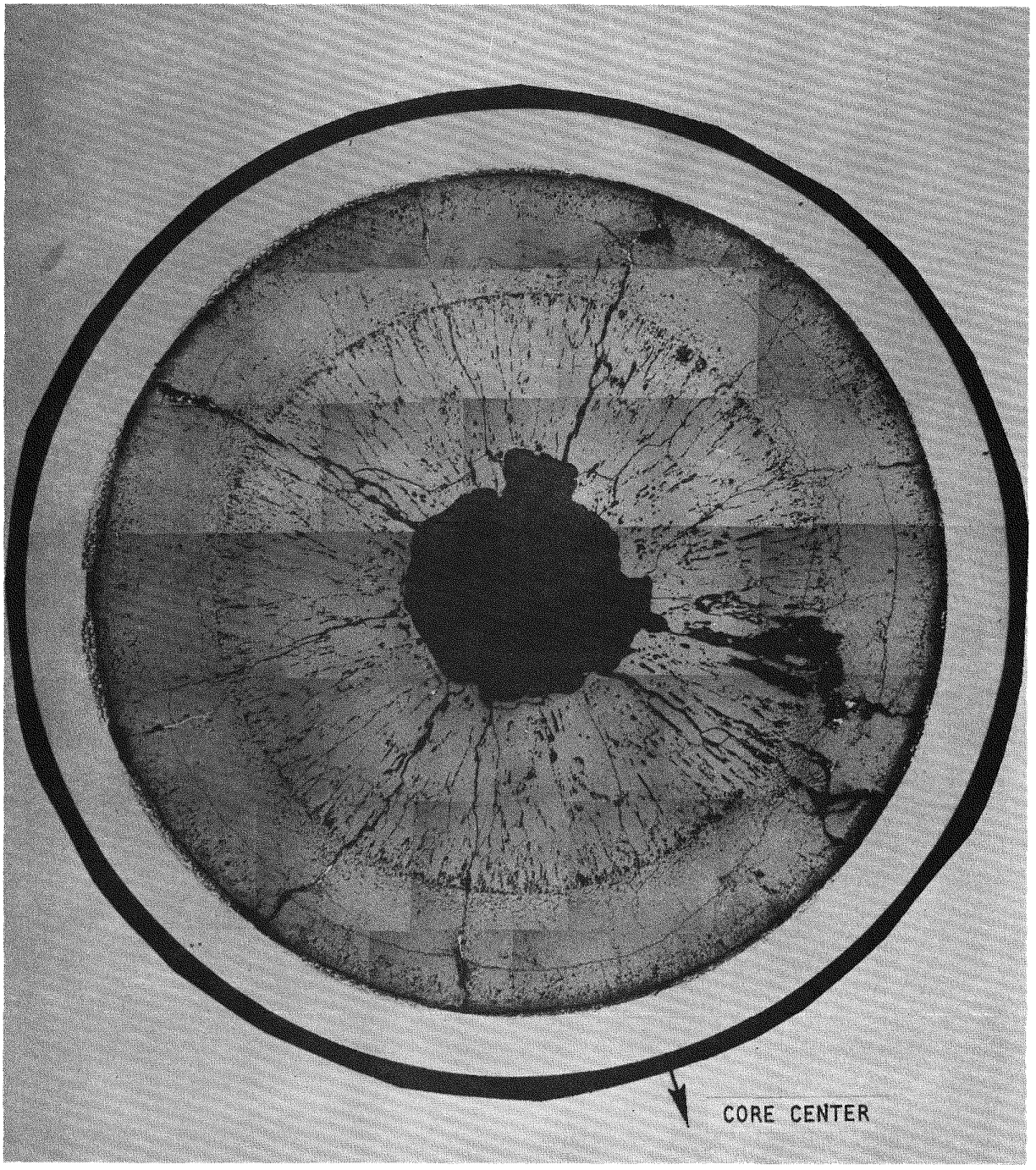

ANL-MSD-168568

Fig. 7.2 Illustration of occurrence of cladding attack between, but not adjacent to, radial cracks in the fuel in rod G-1 (6.7 in. above core bottom; burnup, 6.1 at-%; power, 15.8 kW/ft; cladding inside temperature, 780°C)

ANL-MSD-168682-4 X250

Fig. 7.3 Photograph showing nature of and maximum extent of attack in rod G-1 cladding (6.75 in. above the bottom of core)

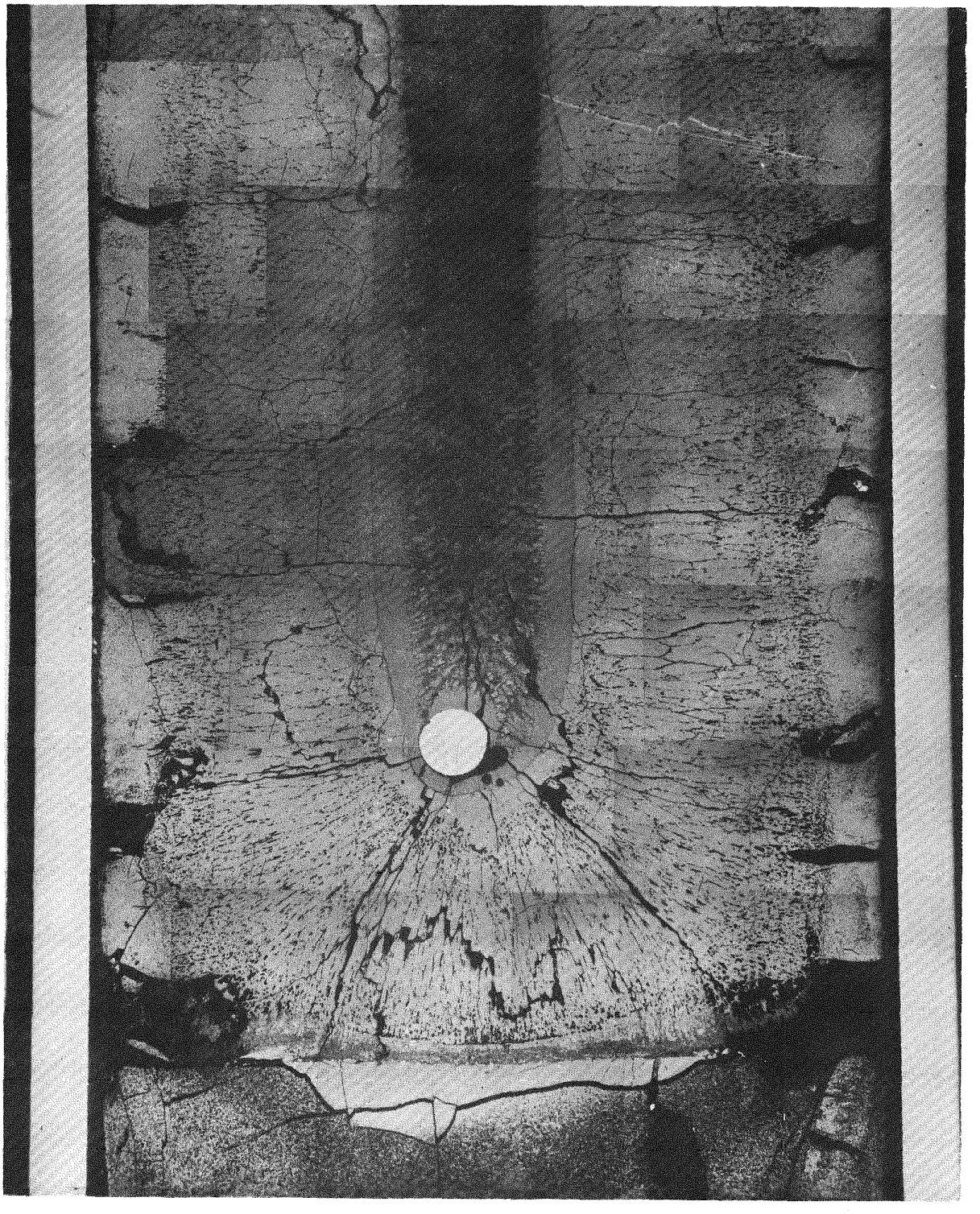

ANL-MSD-168787

Fig. 7.4 Evidence of solidified molten fuel in axial hole near bottom of fuel rod G-1 and closure of bottom of hole by fuel (by vapor transport) (burnup, 5.4 at-%; power, 14.0 kW/ft; cladding inside temperature, 690°C.

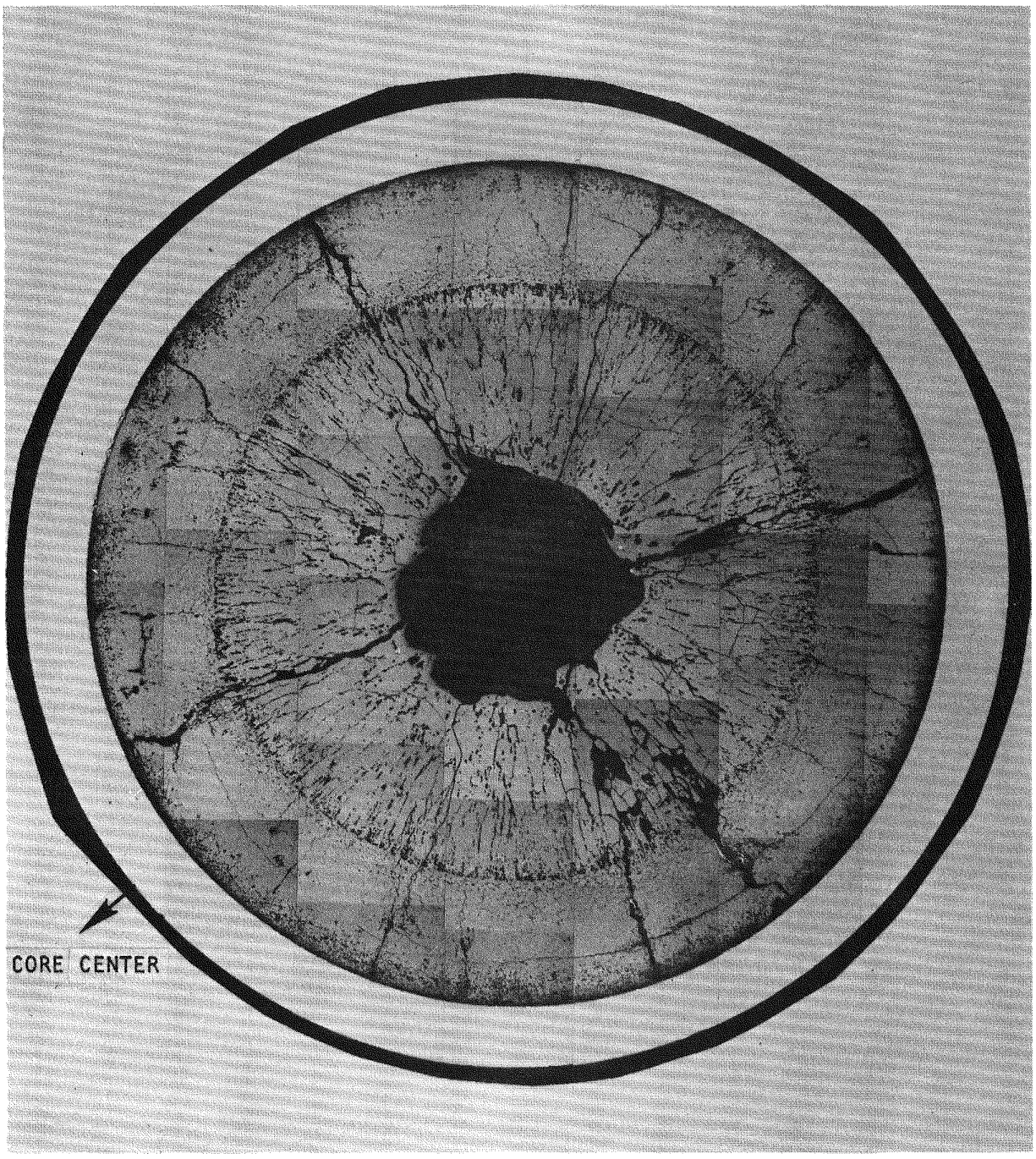

ANL-MSD-168567

Fig. 7.5 Illustration of existence of porosity in the outer periphery of the columnar grain-growth region and high-density equiaxed grain-growth region in rod G-1 (3.3 in. above core bottom; burnup, 5.8 at-%; power, 14.9 kW/ft; cladding inside temperature, 735°C)

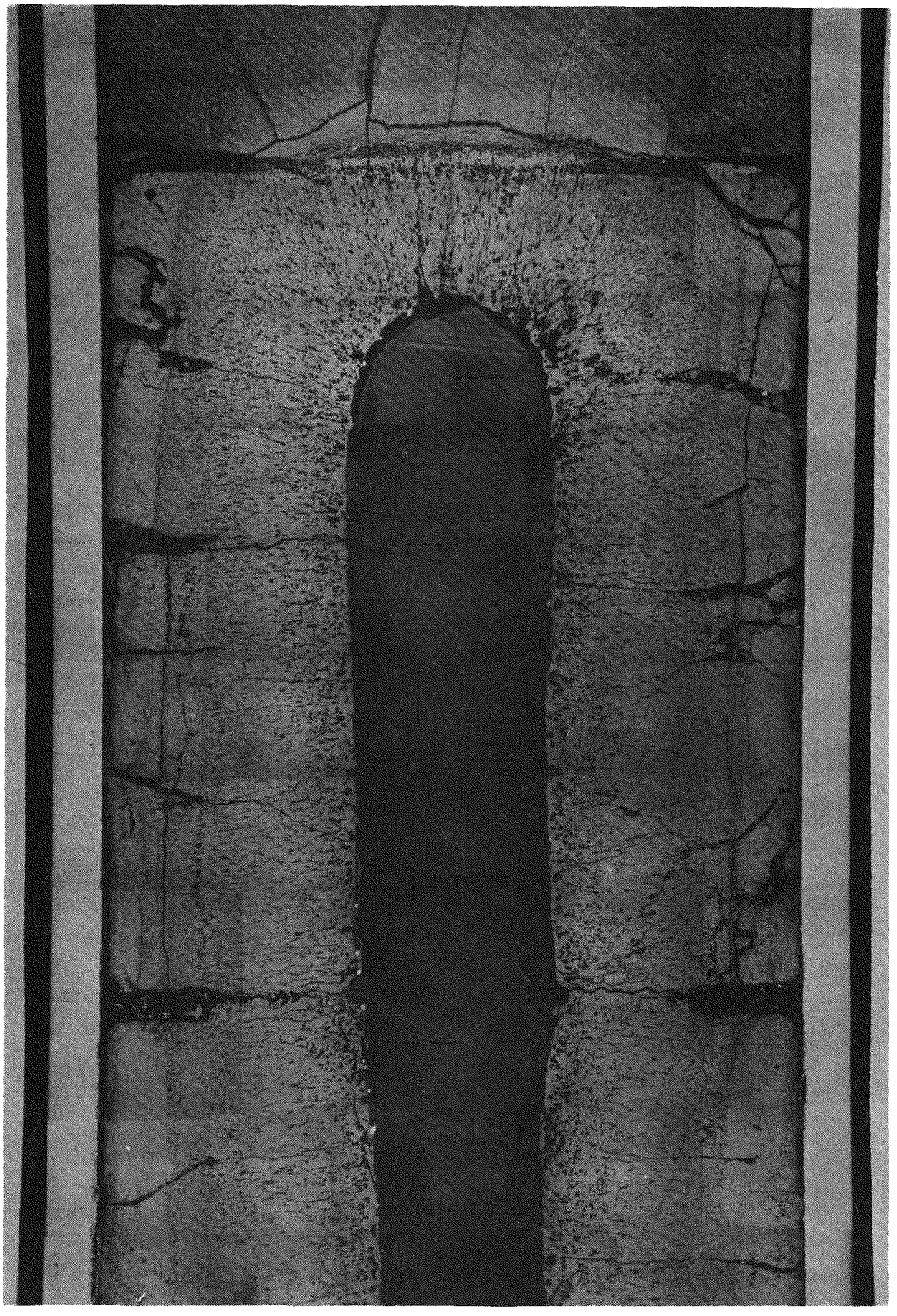

ANL-MSD-168783

Fig. 7.6 Illustration of closure of central hole in rod G-1 by vapor transport of fuel to the upper fuel-blanket pellet interface (burnup, 5.3 at-%; power, 13.7 kW/ft; cladding inside temperature, 785°C)

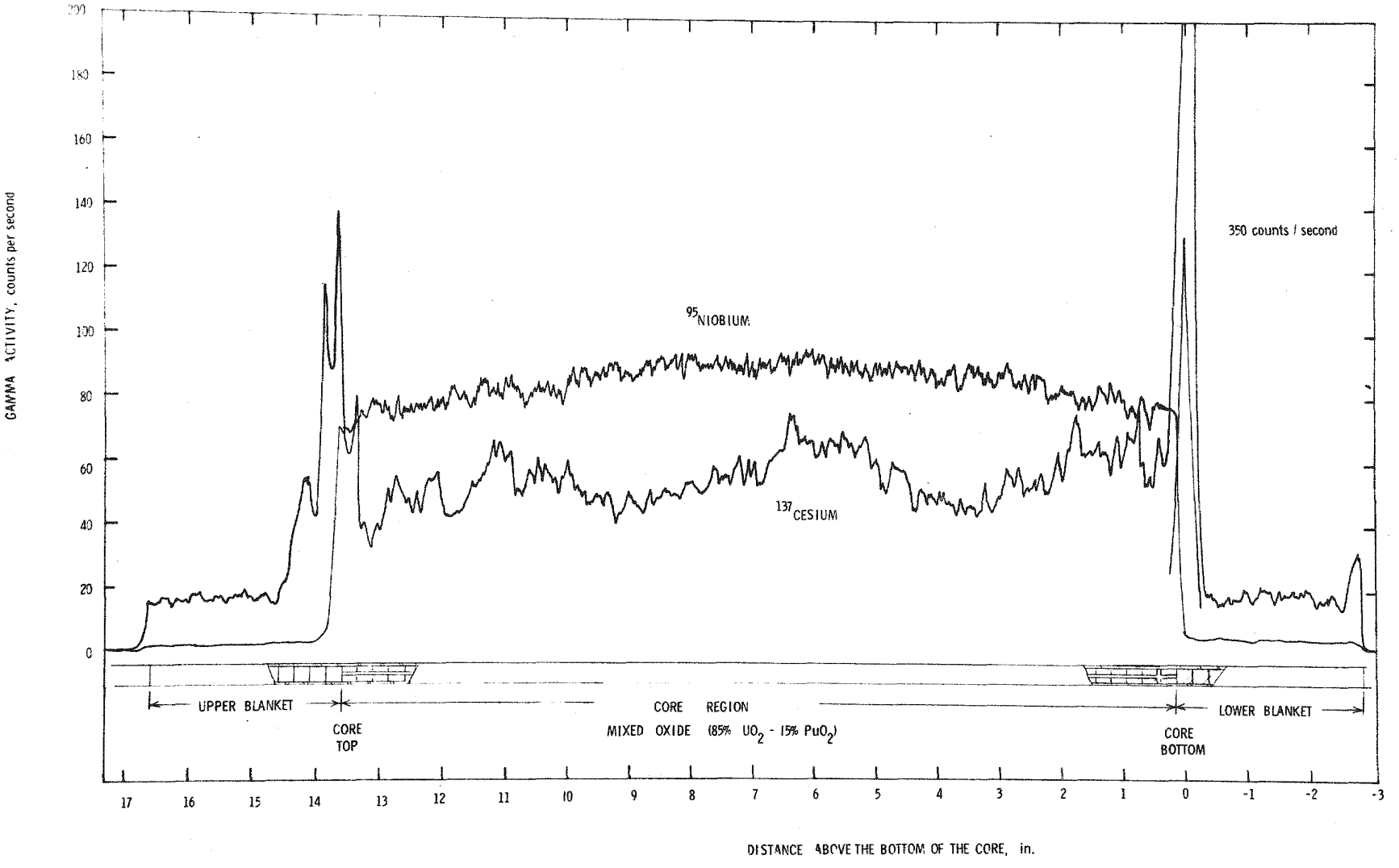

ANL-MSD-168223

Fig. 7.7 Gamma scans of fuel rod G-1 (note large amounts of Cs^{137} activity at both ends of the fuel column, i.e., at both upper and lower fuel-blanket interfaces)

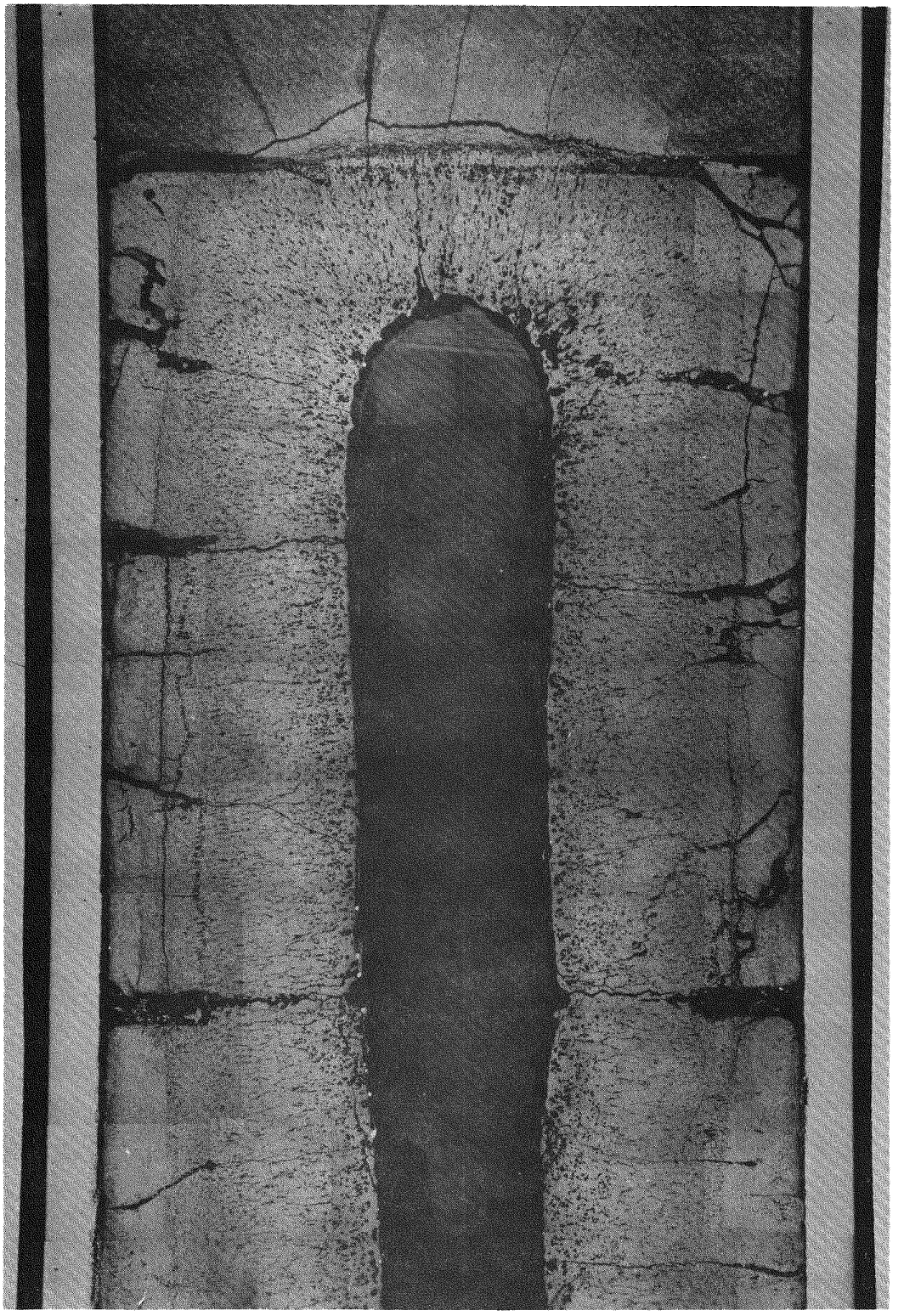

ANL-MSD-168783

Fig. 7.6 Illustration of closure of central hole in rod G-1 by vapor transport of fuel to the upper fuel-blanket pellet interface (burnup, 5.3 at-%; power, 13.7 kW/ft; cladding inside temperature, 785°C)

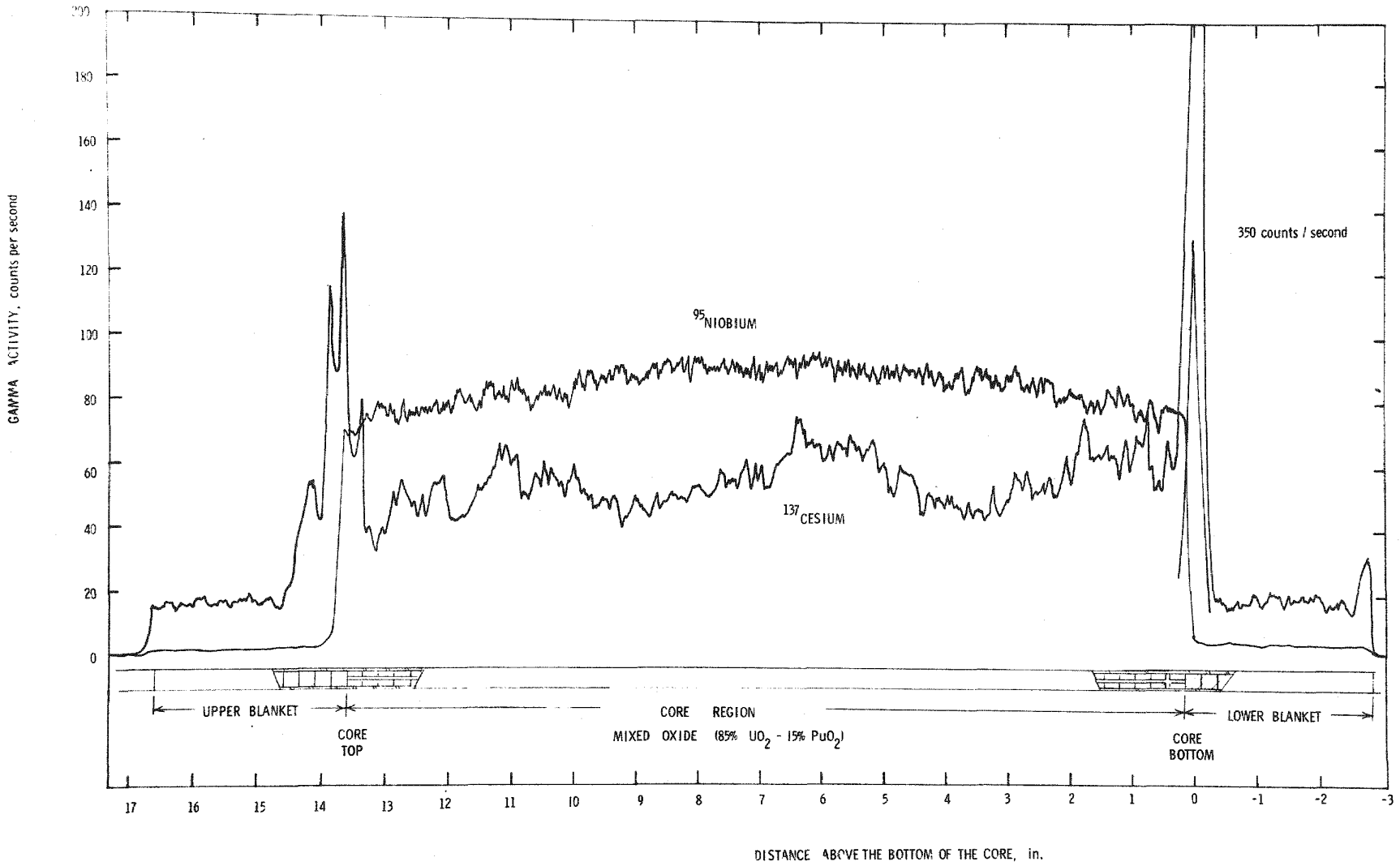

ANL-MSD-168223

Fig. 7.7 Gamma scans of fuel rod G-1 (note large amounts of Cs^{137} activity at both ends of the fuel column, i.e., at both upper and lower fuel-blanket interfaces)

The relative activities of the four representative fission products in the fuel and blanket regions of fuel rods G-1, G-4, and G-8 are given in Table 7.1. These data were obtained from the axial gamma-activity profile for each of the nuclides, as reported previously.[2] However, these relative activities are not directly convertible to relative concentrations. In addition, the fission-product loadings of the interface regions between the fuel and blanket should be considered. Integration of the relative activity levels over the entire length of the fuel and blanket regions yields the fractional amounts of each isotope in each region. These data are given in Table 7.2. Examination of these results indicates that

1. Within the limits of error expected from the measurements, there is no movement of Zr^{95}; this typifies nonvolatile, refractory, fission products.*

2. Regions of enhanced activity of Ba^{140}/La^{140} are not always detected at the fuel-blanket interfaces. This is probably due to the rather large scanning interval of 0.1 in. Previous work[4] has shown that even at scanning intervals of 0.050 in., activity peaks that are seen at closer scanning intervals may not be detected at the larger intervals.

3. There may be movement of the mass-140 chain into the blanket subsequent to plateout at the fuel-blanket interface. However, such movement (if it occurs) is small compared to that observed for iodine and cesium.

4. There is substantial movement of I^{131} into the upper fuel-blanket interface region in all three rods. In addition, rod G-1 also shows 6% of the iodine in the lower fuel-blanket interface region, perhaps because of the higher operating cladding temperature of this rod.

---

*The anomalously high 1.8% of the activity in the upper blanket may be due to integration errors because the axial scan shows no enhanced activity in the blanket region. However, the Ba^{140}/La^{140} and Cs^{137} activities in this region also seem higher than expected. This should be investigated during postirradiation examination.

Table 7.1

RELATIVE ACTIVITIES OF SELECTED FISSION PRODUCTS IN THE FUEL AND BLANKET REGIONS OF F-1 (X094) FUEL RODS

Rod No.	Maximum Outside Cladding Temperature (°C)	Peak Linear Power (kW/ft)	Burnup (MWd/Te)	Ratio of Relative Activities at 50,000 MWd/Te			
				I-131 (blanket) / I-131 (fuel)	Cs-137 (blanket) / Cs-137 (fuel)	Zr-95 (blanket) / Zr-95 (fuel)	Ba/La-140 (blanket) / Ba/La-140 (fuel)
G-1	780	16.1	56,000	0.04	0.45-0.60[a]	0.03	0.04
G-4	680	13.3	52,000	0.04	0.25-0.40[a]	0.04	0.04
G-8	670	13.7	27,000	0.04	0.40	0.02-0.03[a]	0.03-0.04[a]

[a]Ranges indicate the activities in the lower and upper blankets and the adjacent fuel region.

Table 7.2

FISSION-PRODUCT DISTRIBUTION IN FUEL RODS G-1, G-4, AND G-8[a]

FROM INTERIM GAMMA SPECTROMETRY EXAMINATION

(In percent)

Region	Calculated Values[b]	Zr-95			Ba/La-140			I-131			Cs-137		
		G-1	G-4	G-8	G-1	G-4	G-8	G-1	G-4	G-8	G-1	G-4	G-8
Lower blanket	0.5	0.7	0.6	0.6	0.8	0.7	0.6	0.7	0.9	0.7	6.6	3.0	5.4
Lower interface[c]	---	---	---	---	7.0	---	---	6.2	0.04	0.04	11.7	6.1	3.1
Fuel region	99.	98.6	98.8	97.6	90.8	98.7	95.8	81.4	93.8	82.8	64.2	77.2	70.9
Upper interface[c]	---	---	---	---	0.6	---	0.7	11.1	4.4	15.8	10.5	9.9	6.9
Upper blanket	0.5	0.7	0.6	1.8	0.9	0.6	2.9	0.6	0.9	0.7	7.0	3.8	13.7

[a]Rod No.	Burnup (MWd/Te)	Surface Cladding Temperature (°C)
G-1	56,000	780
G-4	52,000	680
G-8	27,000	670

[b]Calculated values are based on fraction of fissions occurring in each region.

[c]The interface regions are of variable length and include the region of "enhanced activity" at the interface.

5. Rod G-8 appears to have exhibited greater I^{131} migration than rod G-4 (at the same cladding temperature) in spite of the lower burnup of rod G-8. Although, this conclusion is reinforced by the behavior of Ba^{140}/La^{140} and Cs^{137}, the further anomalous concentration of 1.8% of the Zr^{95} in the upper blanket of this rod indicates that the calculated operating temperature of rod G-8 should be checked and that special attention should be paid to determining the cause of this behavior during postirradiation examination.

6. Cesium is transported more readily than iodine, as evidenced by the lower retention in the fuel and the higher concentrations in the blanket. The enhanced cesium concentrations are probably due to the transport of each mass chain as the xenon precursor. These conclusions should be confirmed during postirradiation examination of the F-1 (X094) experiment by mass spectrometer analysis for cesium nuclides in the charcoal traps.

7.2.2. Fast-flux Irradiation Experiment F-3

Work continued on the fabrication and assembly of the fuel-rod capsules for the F-3 fast-flux experiment, which has been designed for irradiation in an EBR-II core position (row 4) and which will share a type J19A subassembly with an ANL Group-08 high-temperature chemistry experiment. The initial loading of the subassembly will contain ten F-3 fuel-rod capsules and nine Group-08 fuel-rod capsules. The F-3 fuel rods will achieve neutron exposures up to $\sim 1.5 \times 10^{23}$ nvt at 100,000 MWd/Te burnup. The F-3 fuel-rod cladding temperatures will range from 675°C to 750°C and the linear heat-generating ratings will range from 12 to 15 kW/ft.

The assembly of twelve rods for the F-3 experiment has been completed by ANL. Encapsulation and sodium bonding has been initiated. Fabrication of the F-3-fuel rod capsules is still scheduled for completion in May 1974.

Comments on the design of the subassembly flow strips, which will contain thermocouples, have been received from the EBR-II project. Minor changes have been requested and are being incorporated in a revised design.

7.3. IN-PILE LOOP TEST PROGRAM

In support of the fuel-element development program for the GCFR, an in-pile loop test program is being planned. These in-pile loop tests will provide the information necessary to establish design and safety margins of the GCFR fuel elements and to verify the analytical methods developed. The tests will determine the performance of GCFR fuel-element models during transients at full GCFR power conditions. These transient tests will complement the tests of GCFR vented fuel-rods bundles in the BR-2 helium loop at Mol, Belgium, which are expected to provide information on normal operation and endurance of the rod bundles. Endurance testing requirements are also being considered for the U.S. loop to provide backup capability to supplement the BR-2 loop tests if that should become necessary.

A scoping study to define the costs and schedules for the in-pile loop program has been initiated. The problems to be investigated were defined, loop operational and test requirements were formulated, and a preliminary test program was prepared. Meetings were held with DRRD and with Aerojet General Nuclear Corporation (ANC), who is preparing the scoping study, to discuss the overall programmatic and technical requirements.

Major portions of the tradeoff studies for the loop were completed by ANC and will be included in the In-pile Loop Program Plan. From these tradeoff studies, ANC determined the most suitable conceptual design configuration for the in-pile loop. This loop design is characterized by a relatively high helium inlet temperature to the circulators, a single through-tube, and a single depressurization tank.

The test reactor evaluation was completed by ANC. The ETR is considered to be the most suitable test reactor for the GCFR in-pile loop program. Design and tradeoff studies will continue based on using the ETR as the test reactor.

Drafts of the outlines for the program planning document and the safety assessment report were prepared by ANC and submitted to GA for review. A preliminary draft for the management plan was prepared by GA, which describes the functional relationship between GA, ANC, and DRRD.

REFERENCES

1. "Gas-Cooled Fast Breeder Reactor Quarterly Progress Report for the Period November 1, 1973 through January 31, 1974," USAEC, Report GA-A12894, General Atomic Company, April 12, 1974.

2. "Gas-Cooled Fast Breeder Reactor Quarterly Progress Report for the Period February 1, 1973 through April 30, 1973," USAEC, Report Gulf-GA-A12635, Gulf General Atomic Company, June 15, 1973.

3. "Gas-Cooled Fast Breeder Reactor Quarterly Progress Report for the Period May 1, 1973 through July 31, 1973," USAEC, Report Gulf-GA-A12728, Gulf General Atomic Company, October 10, 1973.

4. "Gas-Cooled Fast Breeder Reactor Quarterly Progress Report for the Period May 1, 1972 through July 31, 1972," USAEC, Report Gulf-GA-A12252, Gulf General Atomic Company, August 31, 1972.

8. TASK 4700—NUCLEAR ANALYSIS AND REACTOR PHYSICS

8.1. CRITICAL EXPERIMENT PLANNING

A joint meeting with members of the ANL Applied Physics Division was held at GA in February to discuss the proposed experimental program. A sequence of six program phases was discussed which progresses from a single large core with uniform "average" enrichment and correct void fraction to a four-zone core having approximately the same zonal enrichments as the 300-MW(e) GCFR but with a reduced void fraction. Phases I through IV correspond to Assembly 1, as designated in the scoping document,[1] whereas Phases V and VI correspond to Assembly 2. Experimental parameters to be measured in each phase were discussed and preliminary experimental priority assignments by phase were made.

Preliminary benchmark specifications for Phase I were generated at ANL; the dimensions of the benchmark critical assembly for use in joint preanalysis are given in Table 8.1 and the homogeneous atom densities for use in unit cell calculations are listed in Table 8.2. The unit cell configuration and arrangement of materials for the core cell is shown in Fig. 8.1.[2]

Preliminary analysis is under way at GA of benchmark calculations for Assembly 1 using GA methodology and ENDF/B, Version III nuclear data. Utilizing the cell configuration shown in Fig. 8.1, two separate two-region cell calculations were performed with the GGC-5 code[3] to accurately account for resonance energy shielding effects. In both cases, the U^{238} in the Pu-U-Mo fuel plate was treated as a distinct and separate nuclide from the U^{238} in the U_3O_8 plate. The first calculation was done in the conventional manner; i.e., the fuel plate was considered Region 1 and everything else in the cell was considered as "moderator" in Region 2. In the second calculation, the U_3O_8 plate was considered as Region 1 and all else, including fuel, was homogenized into Region 2. In this manner, a separate

Table 8.1

BENCHMARK CRITICAL ASSEMBLY EQUIVALENT R-Z DIMENSIONS

Region	Radius[a] (cm)	Half-height (cm)
Core	94.179	61.036
Axial Blanket	94.179	30.480 (thickness)
Radial Blanket	118.646	91.516

[a]Based on ZPR matrix tube cross-sectional area of 30.5201 cm^2.

Table 8.2

HOMOGENEOUS ATOM DENSITIES FOR BENCHMARK UNIT CELLS

(atoms/cm^3 x 10^{-21})

Nuclide	Core	Radial Blanket	Axial Blanket
Pu^{238}	0.00061		
Pu^{239}	0.88435		
Pu^{240}	0.1172		
Pu^{241}	0.0124		
Pu^{242}	0.0019		
U^{234}	0.000044	0.000095	0.000069
U^{235}	0.00915	0.0192	0.0140
U^{236}	0.00021	0.00046	0.00033
U^{238}	4.164	8.9733	6.5203
Am^{241}	0.0080		
O	10.66	17.89	11.32
Cr	2.841	2.413	2.567
Mn	0.195	0.162	0.204
Fe	13.96	8.564	9.097
Ni	1.309	1.095	1.173
Mo	0.2259		

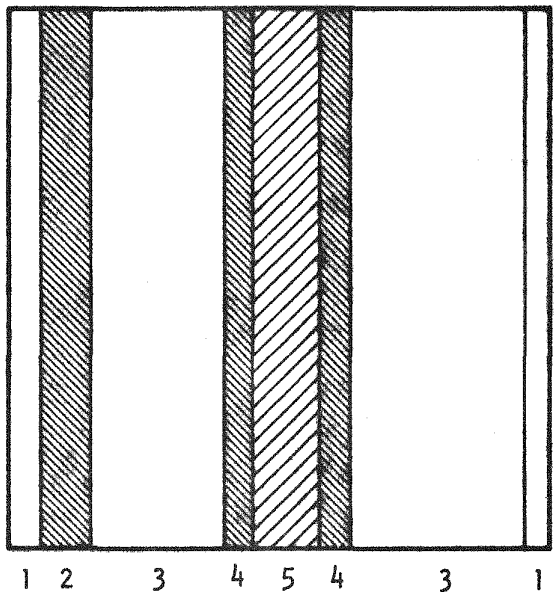

1 - STAINLESS-STEEL MATRIX AND DRAWER
2 - U_3O_8 PLATE
3 - STAINLESS-STEEL VOID CANS
4 - Fe_2O_3 PLATES
5 - Pu-U-Mo FUEL PLATE

Fig. 8.1 Core unit cell representation

set of cross sections for the U^{238} in the U_3O_8 plate was generated for subsequent spatial shielding calculations.

The one-dimensional transport code 1DFX[4] was utilized for computing cell disadvantage factors for energies above the GAROL resolved resonance region, i.e., for groups 1 through 7 of the standard 10-group GA energy mesh. A standard P_1S_{16} transport calculation yielded the disadvantage, or "self-shielding," factors shown in Table 8.3. For comparison, the effect of a higher-order S_N approximation (P_1S_{32}) is also shown. The S_{32} approximation was used for subsequent calculations. For the energy region covered by the GAROL code (groups 8, 9, and 10), the self-shielding is calculated internally in GAROL.

Table 8.3

SPATIAL SELF-SHIELDING FACTORS FOR FUEL REGION IN UNIT CELL

Energy Group	P_1S_{16} Approximation	P_1S_{32} Approximation
1	1.12482	1.17790
2	1.05923	1.08459
3	1.01702	1.02341
4	1.00424	1.00553
5	0.99334	0.99219
6	0.99177	0.99104
7	0.97870	0.97562
8	1.0	1.0
9	1.0	1.0
10	1.0	1.0

A recalculation of the microscopic cross sections with GGC-5 using these spatial self-shielding factors yielded the multigroup cross sections for two-dimensional diffusion calculations.

The ADGAUGE diffusion code[5] was used for the eigenvalue calculations. The shielded core cross sections described above were utilized in the core region. In the blanket regions, the cross sections were averaged over the core spectrum. This procedure is correct for thin blankets and approximately correct for thick blankets. (Future work will delineate the amount of the correction.) Both real and adjoint flux solutions were obtained for central-worth calculations with first-order perturbation (FOP) theory.

To accurately model the experimental configuration, the cross sections used for the central-worth calculations were derived from a totally homogeneous spectrum calculation; i.e., the resonance materials were homogeneously distributed over the unit cell in the calculation rather than being "lumped" in the two-region calculations described above. Such cross sections are appropriate for describing the samples that would be used in making the measurements. For reaction-rate calculations, however, "in-plate" cross sections, i.e., the shielded ones, were utilized to represent the foils that would be used in measurement.

The results of the calculations are given in Table 8.4. The last column of results illustrates the best calculation. The effect of spatial self-shielding is shown by comparison with the second column. Anisotropic neutron diffusion, or "streaming," has not been considered in these calculations.

Table 8.4

PRELIMINARY VALUES FOR PHASE I ASSEMBLY

Quantity Calculated	Resonance Heterogeneities	Resonance and Spatial Heterogeneities
Central worths, $\Delta\rho$/kg (2-D perturbation)		
He	-1.009×10^{-3}	-1.077×10^{-3}
B-10	-2.452×10^{-2}	-2.418×10^{-2}
Fe	-4.903×10^{-5}	-5.209×10^{-5}
U-235	1.326×10^{-3}	1.307×10^{-3}
U-238	-9.254×10^{-5}	-9.384×10^{-5}
Pu-239	1.714×10^{-3}	1.686×10^{-3}
Pu-240	2.560×10^{-4}	2.478×10^{-4}
Reaction-rate ratios		
f^{28}/f^{49}	0.02732	0.02589
C^{28}/f^{49}	0.1455	0.1535
f^{40}/f^{49}	0.2246	0.2307
f^{41}/f^{49}	1.3028	1.2969
$B^{10}(n,\alpha)/f^{49}$	------	1.3264
k_∞ (GAM calculation)	1.5159	1.5248
k_{eff} (2-D calculation)	1.0123	1.0207
Δk_{het}	------	0.0084

Additional eigenvalue calculations were made to determine the critical radius for the benchmark core with no streaming corrections. Eigenvalues as a function of core radius for constant blanket thickness are given in Table 8.5. From these calculations, it is possible to derive edge drawer worths, which are useful in ZPR operations. The substitution worths that would be expected from replacing a matrix drawer (on both sides of the ZPR matrix) with blanket drawers are listed in Table 8.6.

Table 8.5

CRITICAL RADIUS CALCULATION

(Radial Blanket Thickness = 24.4 cm)

Core Radius (cm)	Eigenvalue
94.2	1.02070
91.2	1.01167
87.2	0.99898
87.52	1.0 (interpolated)

Table 8.6

SUBSTITUTION WORTHS FOR REPLACING CORE EDGE DRAWERS WITH BLANKET MATERIAL

Average Radius (cm)	Equivalent Number of Drawers	$\Delta\rho$	$\Delta\rho$/Drawer
92.7	57.25	8.745×10^{-3}	1.527×10^{-4}
89.2	73.45	12.556×10^{-3}	1.710×10^{-4}

An initial series of calculations has been made of the simulation of steam entry in the Phase I critical assembly. Two-region GGC-5 spectral calculations have been made for the unit cell (1) with 0.052 g/cm^3 H_2O and (2) with the same hydrogen density in the form of H_2C (polyethylene) in the void can interiors. A comparison of the spectra exhibited virtually no difference in the substitution of carbon for oxygen. The unit cell (GAM)

k-infinity value for the H_2O and H_2C simulation of steam was 1.3410 and 1.3312, respectively. The expected decrease from the 1.5248 value for the dry case indicates the anticipated negative effect of steam entry on the system multiplication.

REFERENCES

1. Moore, R. A., "A Critical Experiment Program for the 300-MW(e) Gas-Cooled Fast Breeder Reactor - Scope and Purpose," USAEC, Report Gulf-GA-A12780, Gulf General Atomic, October 1973.

2. Private Communication, J. E. Marshall, Argonne National Laboratory.

3. Mathews, D. R., et al., "GGC-5, A Computer Program for Calculating Neutron Spectra and Group Constants," Gulf General Atomic, Report GA-8871, September 1971.

4. Archibald, R., et al., "1DFX - A Revised Version of the 1DF (DTF-IV) SN Transport Theory Code," Gulf General Atomic, Report Gulf-GA-B10820, September 1971.

5. Haschke, D., and U. Nyffenegger, "The Nuclear Design Codes ADGAUGE and STOER," Eidgenössiches Institut für Reaktorforschung Würenlingen, EIR Report 199, May 1971.